Chemistry–A European Journal

Supporting Information

Electron Storage Capability and Singlet Oxygen Productivity of a Ru^{II} Photosensitizer Containing a Fused Naphthaloylenebenzene Moiety at the 1,10-Phenanthroline Ligand

Yingya Yang[+],[a] Jannik Brückmann[+],[a] Wolfgang Frey,[b] Sven Rau,[a] Michael Karnahl,*[b] and Stefanie Tschierlei*[a, c]

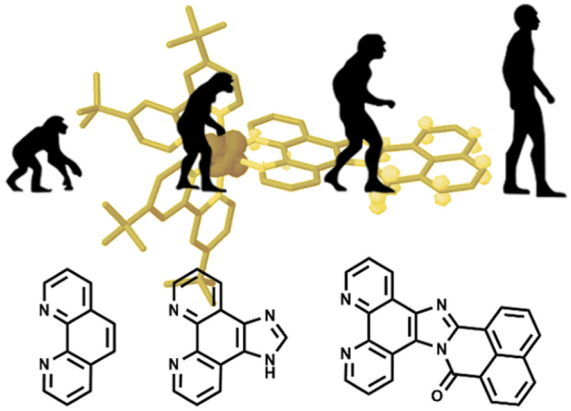

Supporting Information - Table of Contents

1 Experimental Details

NMR spectroscopy. Nuclear magnetic resonance (NMR) spectra were measured at 298 K with different Bruker Avance spectrometers operating at Larmor frequencies of 400 MHz or 500 MHz (^{1}H) and 101 MHz or 126 MHz (^{13}C) and processed with MestreNova software (version 12.0.0). All spectra were referenced to the deuterated solvent as an internal standard.[1] Chemical shifts are given by the residual solvent proton signal. Coupling constants *J* are presented as absolute values in Hz, without considering the kind of the coupling. For the characterization of the NMR signals the following abbreviations are used: d = doublet, m = multiplet, dd = doublet of doublets, dt = doublet of triplets and td = triplets of doublets.

Mass spectrometry. Mass spectrometric (MS) measurements were performed by the analytical service of the Institute of Organic Chemistry at the University of Stuttgart. High resolution mass spectra were measured using electrospray ionization (ESI) on a Bruker Daltonics micrOTOF-Q. MS values are given as *m/z*.

X-ray analysis. Crystals suitable for X-ray crystallography were mounted using a MicroLoop and Perfluoropolyalkylether (viscosity 1800 cSt). X-ray diffraction intensity data were measured at 150 K on an Agilent SuperNova CCD single crystal diffractometer with an Atlas detector using Cu-Kα radiation (wavelength λ = 1.5406 Å). The structure of **Rubiipo** was solved by direct methods using SHELXL97 software. ORTEP molecular graphics were performed by XP software.[2] CCDC 1993565 (**Rubiipo**) contains the supplementary crystallographic data for this paper. These data can be obtained free of charge by the Cambridge Crystallographic Data Centre via www.ccdc.cam.ac.uk/data_request/cif or by emailing data_request@ccdc.cam.ac.uk or by contacting The Cambridge Crystallographic Data Centre, 12 Union Road, Cambridge CB2 1EZ, UK.

Infrared spectroscopy. Infrared spectra (IR) were measured by the analytical service of the Institute of Organic Chemistry at the University of Stuttgart using a Bruker ALPHA IR spectrometer in ATR (attenuated total reflection) modus. The location of the IR signals is given in wavenumbers.

Steady-state absorption and emission spectroscopy. Steady-state UV/vis absorption spectra were recorded with a JASCO V-670 spectrophotometer and emission spectra were measured with a JASCO FP-8500 spectrofluorometer. For measurements under air in acetonitrile, ROTISOLV®, UV/IR grade solvents purchased from Carl Roth were used. Quantum yields were determined from the integrated area of emission in comparison to $[Ru(bpy)_3](PF_6)_2$ as reference compound ($\Phi = 0.06$ in degassed acetonitrile[3]), detected at an excitation wavelength of 441 nm.

Photostability tests. UV/vis absorption spectra were recorded with an Avantes AvaSpec-ULS2048CL spectrophotometer. For irradiation in the UV/vis range a Xe arc lamp (150 W) from LOT Quantum Design was used. The measurements were carried out both under aerated and oxygen free conditions. For the latter, degassed acetonitrile was used. The samples were prepared using the same method as for the absorption and emission measurements applying sealed quartz glass cuvettes with a pathlength of 10 mm.

Nanosecond transient absorption spectroscopy. A Q-switched pulsed Nd:YAG laser (Q-smart 450mJ, Quantel laser) was used to generate excitation pulses with an output centered at 355 nm (approx. 6 ns pulse duration. repetition rate of 10 Hz). These pulses were passed through a laser line filter (CWL = 355 ± 2 nm, FWHM = 10 ± 2 nm) to ensure that the samples were only excited by 355 nm light. The power of the pump beam was about 3 mJ per pulse at the sample. The stability of the sample was verified by means of UV/Vis spectra before and after each measurement. The spectrometer used was a LP980-K spectrometer

[1] H. E. Gottlieb, V. Kotlyar, A. Nudelman, *J. Org. Chem.*, **1997**, 62, 7512-7515.
[2] G. M. Sheldrick, *Acta Crystallogr. C*, **2015**, 71, 3-8.
[3] J. V. Caspar, T. J. Meyer, *J. Am. Chem. Soc.* **1983**, *105*, 5583-5590.

from Edinburgh Instruments, where the pump and probe beams spatially overlapped at the sample position in a perpendicular beam setup. The probe lamp was operated in flash mode (150 W ozone-free xenon arc lamp, 30 A), and after passing the sample the probe light was recorded using a photo multiplier tube (Hamamatsu R928P). A standard fused silica cuvette with a layer thickness of 10 mm and a sample OD of approximately 0.3 at the pump wavelength was used in this setup. The compound **Rubiipo** was dissolved in acetonitrile (Carl Roth, ROTISOLV®, UV/IR grade solvents) under inert conditions.

Emission lifetime measurements were performed using a Q-switched pulsed Nd:YAG laser (Q-smart 450 mJ, Quantel laser) with pulse durations of approx. 6 ns at a repetition rate of 10 Hz. As excitation pulses the Nd:YAG output centred at 355 nm were used. Afterwards, the excitation light additionally passed a laser line filter (CWL = 355 ± 2 nm, FWHM = 10 ± 2 nm) to ensure that the samples were only excited by 355 nm. The power of the pump beam was about 1.1 mJ per pulse at the sample and a sample OD of approximately 0.1 at the pump wavelength was used. The emission lifetime of the samples was measured at their respective emission maxima. The emitted light was recorded using a photo multiplier tube of the LP980 spectrometer (Edinburgh Instruments).

Cyclic voltammetry. Cyclic voltammograms were measured in acetonitrile solution with 0.1 M Bu_4NPF_6 as the supporting electrolyte. The measurements were performed with an Autolab potentiostat PGSTAT204 from Metrohm using a three-electrode configuration. As working electrode a glassy carbon disc with a 3 mm diameter stick and as counter electrode a Pt electrode was used. As reference electrode a non-aqueous Ag/Ag^+ electrode (0.01 M $AgNO_3$ in acetonitrile) was utilized with the ferrocene/ferricenium (Fc/Fc^+) couple as reference, added to the solution after each measurement. Thus, all potentials are reported versus the Fc/Fc^+ couple. All scan rates are 0.1 V/s unless otherwise noted.

Singlet Oxygen Evolution Measurements. For the detection of singlet oxygen mixtures of 9,10-anthracenediyl-bis(methylene)dimalonic acid (ABDA) in phosphate buffered solution (PBS) (50 eq.) and the respective Ru(II) complex, *i.e*. **Rubiipo** ($[(tbbpy)_2Ru(biipo)](Cl)_2$), **Rubpy** ($[Ru(bpy)_3](Cl)_2$) or **Ruphen** ($[(tbbpy)_2Ru(phen)](Cl)_2$) in water (1 eq.), were irradiated with a blue custom-made LED-stick (Ulm University, 470 nm, 50 $mWcm^{-2}$). During irradiation UV/vis absorption spectra were continuously detected (every 5 minutes) with a JASCO V-670 spectrophotometer. The sealed quartz glass cuvette with a pathlength of 10 mm was cooled during irradiation by using a custom-made air-cooling apparatus.[4]

DFT calculations. Calculations at the density functional theory (DFT) level were performed using the ORCA program package (Version 4.1.2).[5] For geometry optimizations of the electronic ground state, the BP86 exchange-correlation functional was used.[6] Excited state calculations were carried out with the B3-LYP functional, starting from ground state structures optimized with the B3-LYP functional.[7] To account for dispersion effects, the DFTD3 V3.1 correction (D3) by S. Grimme including the Becke-Johnson (BJ) damping is used throughout all B3LYP calculations.[8] As basis sets the triple zeta valance plus polarization functions (def2-TZVP) were used.[9] Solvation effects were accounted for by the conductor-like polarizable continuum model, CPCM, with an appropriate dielectric constant and refractive index of acetonitrile.[10]
All stationary points on the potential energy surface of the S_0 state were verified by calculations of the energy second derivatives with respect to nuclear coordinates. For the calculation of excited states at the time-dependent density functional theory level, the Tamm-Dancoff approximation (tda-TD-DFT) was used.

---

4 M. G. Pfeffer, T. Kowacs, M. Wächtler, J. Guthmuller, B. Dietzek, J. G. Vos, S. Rau, *Angew. Chem. Int. Ed.*, **2015**, 54, 6627-6631.

5 a) F. Neese, *WIREs Comput. Mol. Sci.*, **2017**, 8. b) F. Neese, *Interdiscip. Rev. Comput. Mol. Sci.*, **2012**, 2, 73.

6 a) K. Eichkorn, O. Treutler, H. Öhm, M. Häser and R. Ahlrichs, *Chem. Phys. Lett.*, **1995**, 242, 652-660. b) F. Weigend, *Phys. Chem. Chem. Phys.*, **2006**, 8, 1057-1065.

7 O. Treutler, R. Ahlrichs, *J. Chem. Phys*., **1995**, 102, 346-354.

8 a) S. Grimme, J. Antony, S. Ehrlich, H. Krieg, *J. Chem. Phys.*, **2010**, 132, 154104. b) S. Grimme, S. Ehrlich, L. Goerigk, *J. Comput. Chem.*, **2011**, 32, 1456.

9 F. Weigend, R. Ahlrichs, *Phys. Chem. Chem. Phys.,* **2005**, 7, 3297-3305.

10 V. Barone, M. Cossi, *J. Phys. Chem. A*, **1998**, 102, 1995.

Visualizations of the B3-LYP molecular orbitals and of the electron density difference maps were made with IboView v20150427 and Jmol, respectively.[11,12]

[11] G. Knizia, *J. Chem. Theory Comput.*, **2013**, 9, 4834-4883.

[12] http://www.jmol.org/

2 Synthetic Details

Unless noted otherwise, all chemicals were commercially available and used without further purification. All solvents of technical grade were distilled by a rotary evaporator prior to use. Solvents of higher quality grade were used without further purification. The following chemicals and precursors were prepared according to literature procedures: 5,6-diamino-1,10-phenanthroline,[13,14] $[(tbbpy)_2RuCl_2]$,[15] 4,4´-di-*tert*-butyl-2,2´-bipyridine (tbbpy)[16,17] and $[Ru(Cl)_2(cod)]_n$.[18] Column chromatography was performed using Silica Gel 60 with dichloromethane or dichloromethane/methanol mixtures.

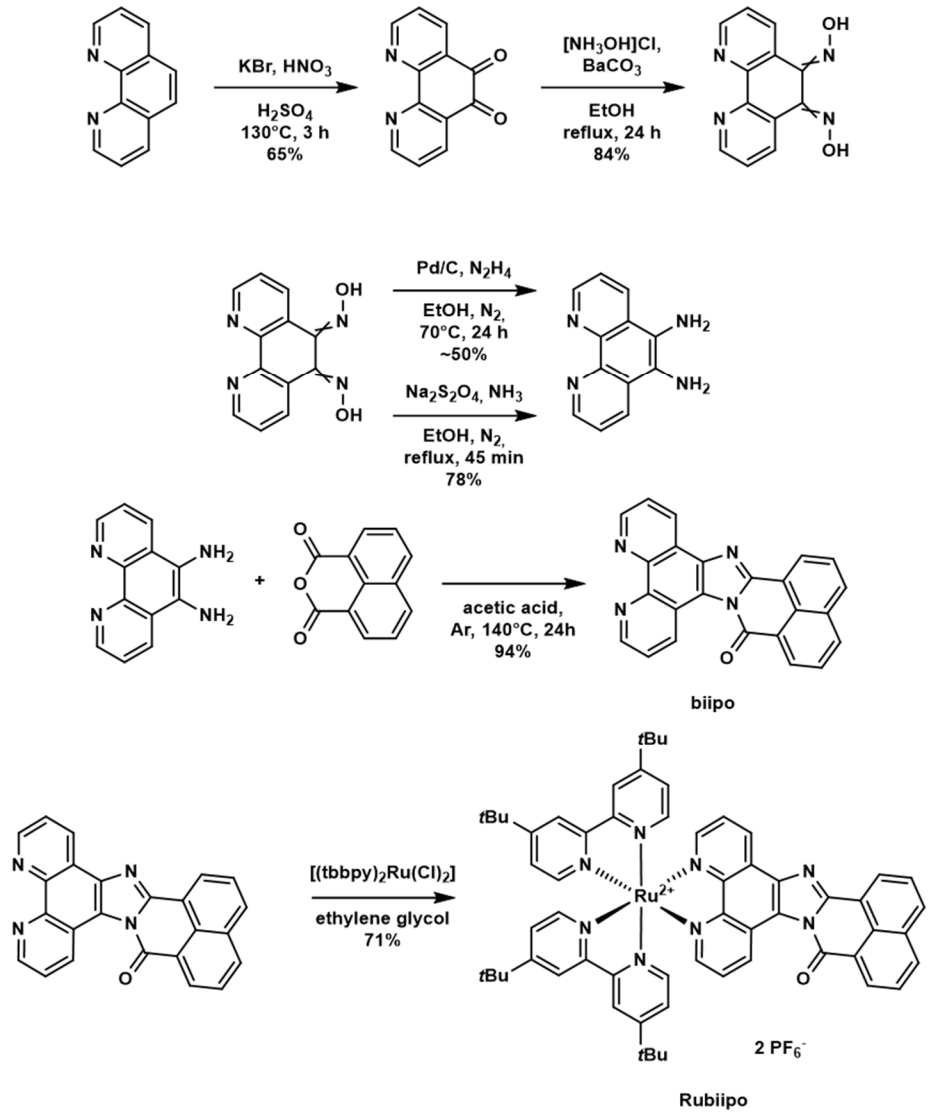

Figure S2.1. Overview of the four-step synthesis of the **biipo** ligand and its corresponding Ru(II) complex **Rubiipo**.

[13] M. N. Jackson, S. Oh, C. J. Kaminsky, S. B. Chu, G. Zhang, J. T. Miller, Y. Surendranath, *J. Am. Chem. Soc.*, **2018**, 140, 1004-1010.

[14] P. Comba, R. Krämer, A. Mokhir, K. Naing, E. Schatz, *Eur. J. Inorg. Chem.*, **2006**, 4442-4448.

[15] M. Hissler, W. B. Connick, D. K. Geiger, J. E. McGarrah, D. Lipa, R. J. Lachicotte, R. Eisenberg, *Inorg. Chem.*, **2000**, 39, 447-457.

[16] P. Belser, A. V. Zelewsky, *Helv. Chim. Acta,* **1980**, 63, 1675-1702.

[17] T. Hadda, H. L. Bozec, *Polyhedron*, **1988**, 7, 575-577.

[18] M. Bennett, G. Wilkinson, *Chem. Ind.*, **1959**, 48, 1516-1516.

Synthesis of 16H-benzo[4',5']isoquinolino[2',1':1,2]imidazo[4,5-f][1,10]phenanthrolin-16-one (biipo): 5,6-Diamino-1,10-phenanthroline (63 mg, 0.30 mmol, 1 eq.) and a slight excess of 1,8-naphthalic anhydride (84 mg, 0.42 mmol, 1.4 eq.) were mixed under argon in 5 mL of acetic acid which was degassed with argon. This mixture was then heated for 24 hours at 140°C. After addition of water, the ligand began to precipitate and was then filtered off. Subsequently, the ligand was thoroughly washed with a saturated, aqueous solution of sodium carbonate, water, ethanol and diethyl ether. Recrystallisation in ethanol gave a yellow solid in good yield (104 mg, 0.28 mmol, 94 %).

^{1}H NMR (300 MHz, $CDCl_3$) **δ** 10.78 (dd, *J* = 8.9, 1.2 Hz, 1H), 9.54 (dd, *J* = 8.4, 1.3 Hz, 1H), 9.34 (td, *J* = 5.2 Hz, 2H), 9.19 (dd, *J* = 7.5, 0.8 Hz, 1H), 9.14 (dd, *J* = 7.5, 1.1 Hz, 1H), 8.62 (d, *J* = 8.4 Hz, 1H), 8.53 (dd, *J* = 8.2 Hz, 1H), 8.40 (dd, *J* = 8.9, 5.1 Hz, 1H), 8.30 (dd, *J* = 8.4, 4.8 Hz, 1H), 8.10 (dt, *J* = 9.3, 7.9 Hz, 2H) ppm. **^{13}C NMR** 159.73, 151.38, 150.49, 145.15, 145.01, 139.37, 138.19, 137.45, 136.99, 136.81, 136.13, 132.53, 132.22, 131.67, 129.19, 128.90, 128.12, 126.75, 126.40, 123.92, 121.65, 120.76, 120.66, 114.16. **HRMS** (ESI): m/z = 373.1061 (found); 373.1084 $[M+H]^+$ (calcd). **IR**: 1700.6 cm^{-1} (C=O stretch, strong).

Synthesis of $[(tbbpy)_2Ru(biipo)][PF_6]_2$ (Rubiipo): The **biipo** ligand (27 mg, 0.07 mmol, 1 eq.) and $[(tbbpy)_2Ru(Cl)_2]$ (58 mg, 0.08 mmol, 1.15 eq.) were mixed in 4 mL of degassed ethylene glycol and heated at 120 °C for 20 hours. After cooling, an aqueous solution of ammonium hexafluorophosphate (20 eq.) was added for precipitation of the desired product. Filtration with a glass frit was followed by washing with water and diethylether. The red precipitate was purified by silica column chromatography with pure dichloromethane and afterwards dichloromethane/methanol (9:1, *v*/*v*). Further purification by changing the anion to chloride and back to hexafluorophosphate yielded 66 mg (0.05 mmol, 71%) of **Rubiipo**.

^{1}H NMR (400 MHz, Acetonitrile-d_3) **δ** 10.11 (dd, *J* = 8.8, 1.2 Hz, 1H), 9.14 (dd, *J* = 8.2, 1.3 Hz, 1H), 8.90 (dd, *J* = 7.3, 1.1 Hz, 1H), 8.85 (dd, *J* = 7.4, 1.1 Hz, 1H), 8.58 – 8.52 (m, 3H), 8.50 (d, *J* = 2.0 Hz, 2H), 8.43 – 8.34 (m, 1H), 8.14 (dd, *J* = 5.3, 1.3 Hz, 1H), 8.06 (dd, *J* = 5.2, 1.3 Hz, 1H), 8.01 – 7.91 (m, 2H), 7.86 (dd, *J* = 8.2, 5.3 Hz, 1H), 7.80 (dd, *J* = 8.8, 5.2 Hz, 1H), 7.75 – 7.65 (m, 2H), 7.54 (d, *J* = 6.1 Hz, 1H), 7.51 – 7.45 (m, 3H), 7.27 – 7.18 (m, 2H), 1.49 (s, 9H), 1.49 (s, 9H), 1.38 (s, 9H), 1.37 (s, 9H) ppm. **^{13}C NMR** (101 MHz, Acetonitrile-d_3) δ 163.52, 163.43, 157.86, 157.74, 152.86, 152.07, 151.93, 151.81, 151.30, 148.15, 147.43, 137.43, 136.18, 134.02, 133.65, 132.64, 131.76, 128.61, 128.37, 127.30, 126.83, 126.06, 125.58, 125.50, 125.38 , 122.45, 122.35, 122.33, 36.22, 36.12, 30.37, 30.26 ppm. **HRMS** (ESI): m/z = 505.1968 (found); 505.20 $[M-2PF_6]^{2+}$ (calcd). **Anal. Calcd**. for $C_{60}H_{60}F_{12}N_8OP_2Ru \bullet 1\ H_2O$: C: 55.43; H: 4.65; N: 8.62; found: C: 55.47; H: 4.69; N: 8.30. **IR**: 1708.2 cm^{-1} (C=O stretch, strong).

3 Structural Characterization of biipo and Rubiipo

3.1 NMR Spectra

The **biipo** ligand and its corresponding Ru(II) complex **Rubiipo** were characterized by ^{1}H and ^{13}C NMR spectroscopic measurements (Figures S3.1 - S3.5). The assignment of the proton signals for **Rubiipo** was further supported by $^{1}H,^{1}H$-COSY experiments (Figure S3.5).

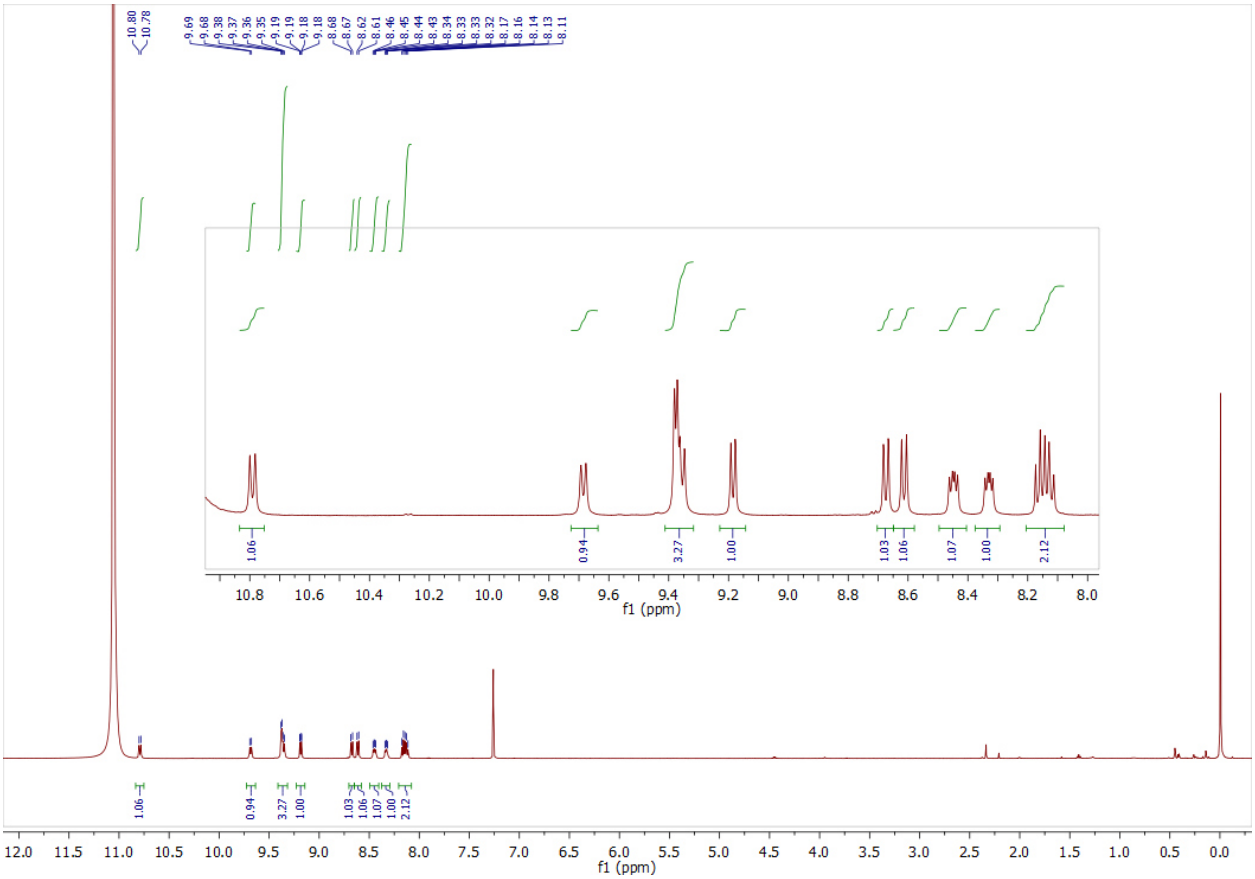

Figure S3.1. ^{1}H NMR spectrum of **biipo** in $CDCl_3$-d.

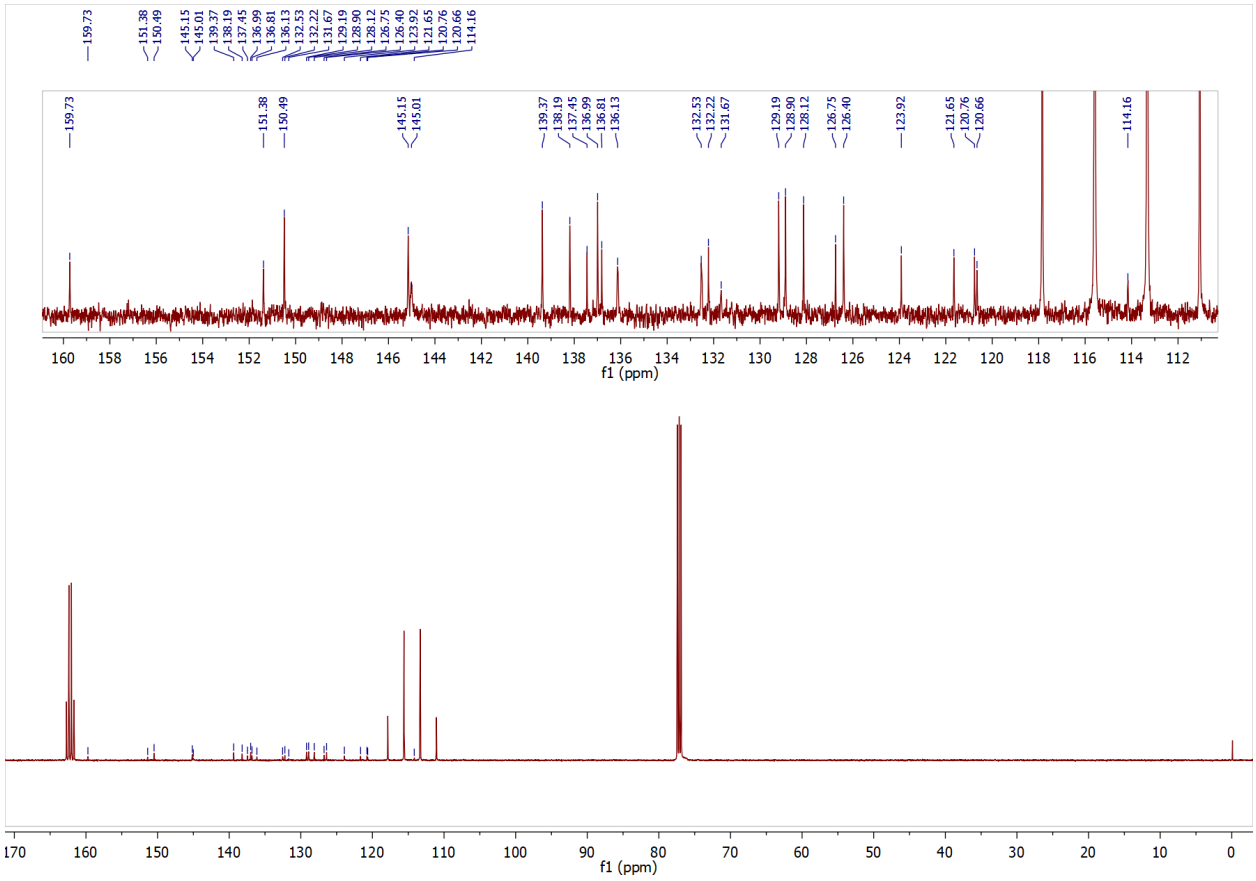

Figure S3.2. ^{13}C NMR spectrum of **biipo** in $CDCl_3$-d with one droplet of trifluoroacetic acid (TFA).

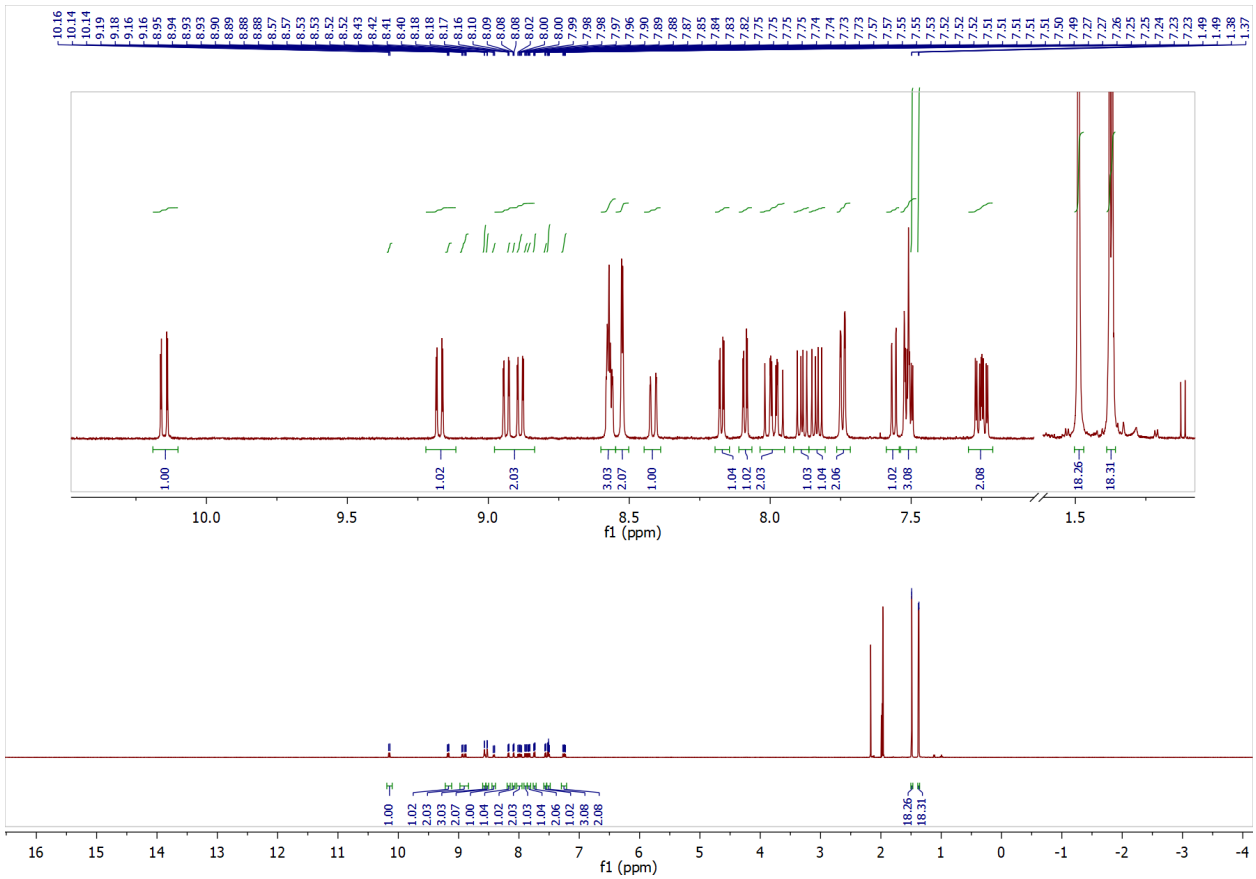

Figure S3.3. ^{1}H NMR spectrum of **Rubiipo** in CD_3CN-d3.

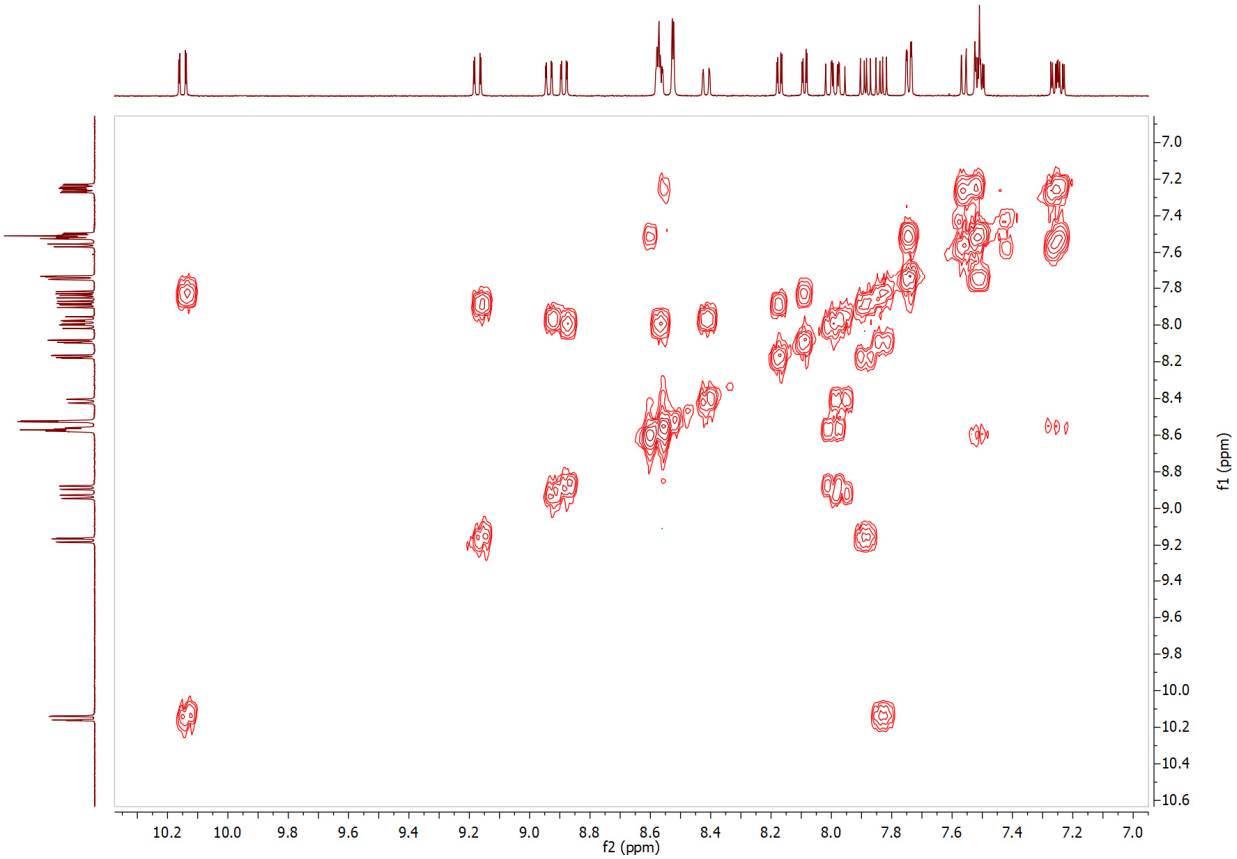

Figure S3.4. H,H COSY spectrum of **Rubiipo** in CD_3CN-d3.

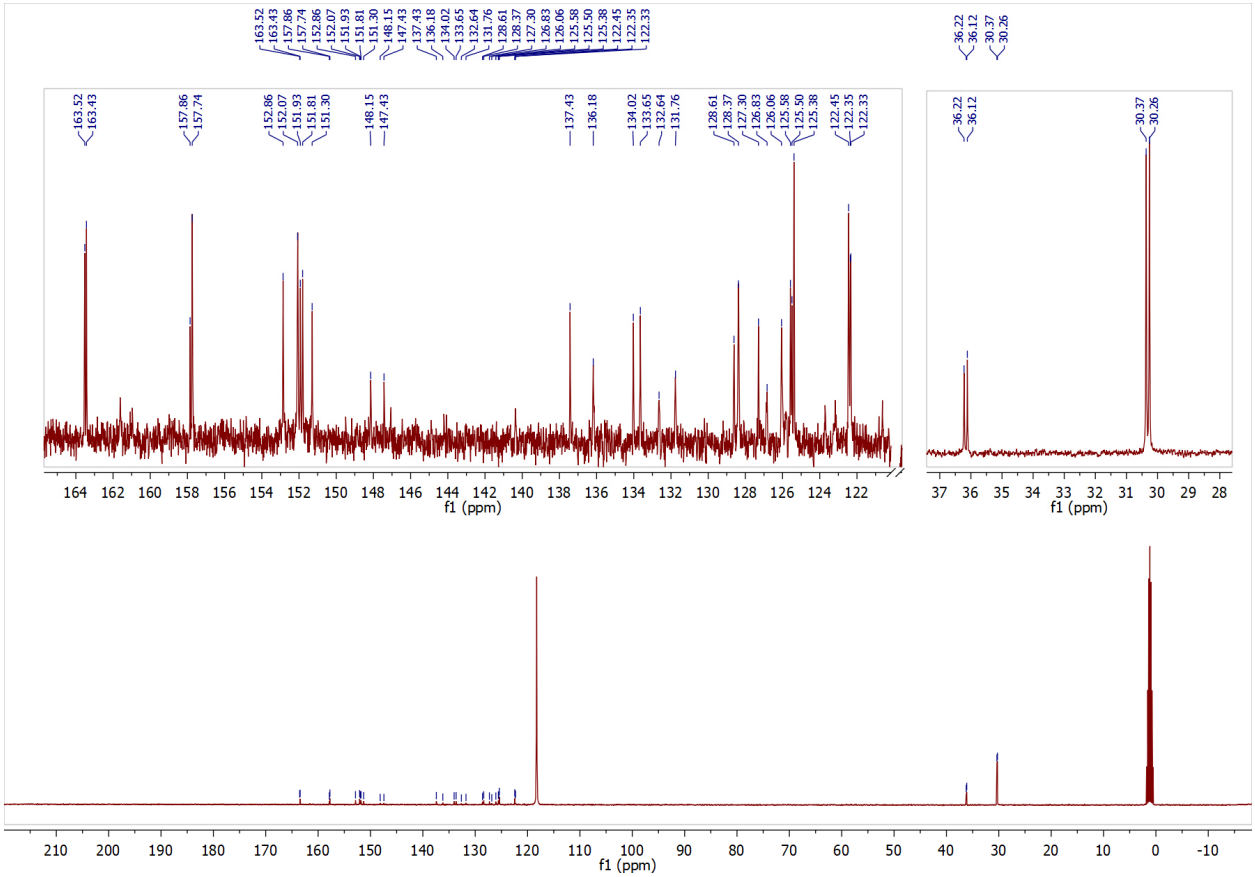

Figure S3.5. ^{13}C NMR spectrum of **Rubiipo** in CD_3CN-d3.

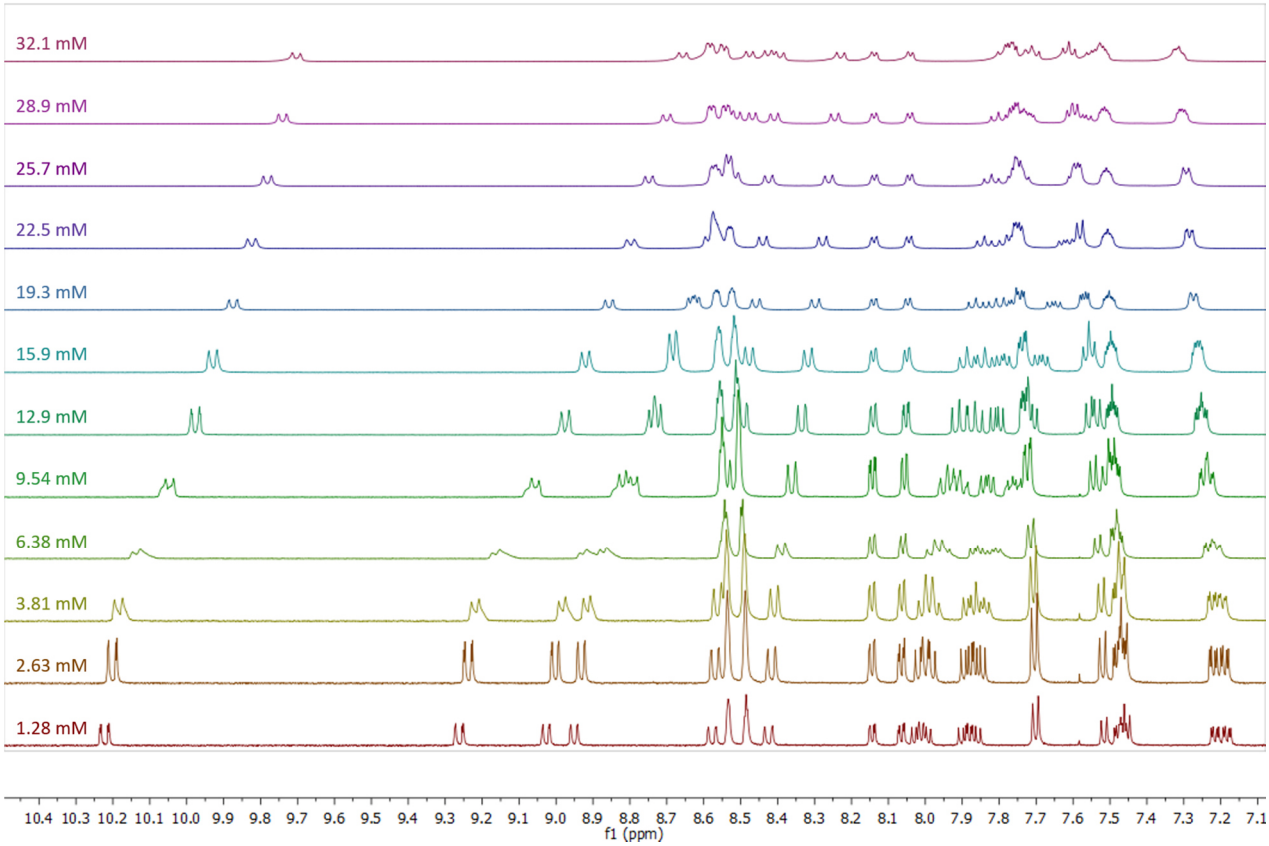

Figure S3.6. Aromatic region of the concentration dependent ^{1}H NMR spectra of **Rubiipo** measured in CD_3CN-d3 at room temperature.

Using this NMR data the investigation and calculation of the dimerization constant of **Rubiipo** (27 M^{-1}) was done like in previous publications (see below).[19,20]

[19] M. G. Pfeffer, C. Pehlken, R. Staehle, D. Sorsche, C. Streb, S. Rau, *Dalton Trans.* **2014**, *43*, 13307-13315.

[20] F. L. Huber, D. Nauroozi, A. K. Mengele, S. Rau, *Eur. J. Inorg. Chem*. **2017**, *34*, 4020-4027.

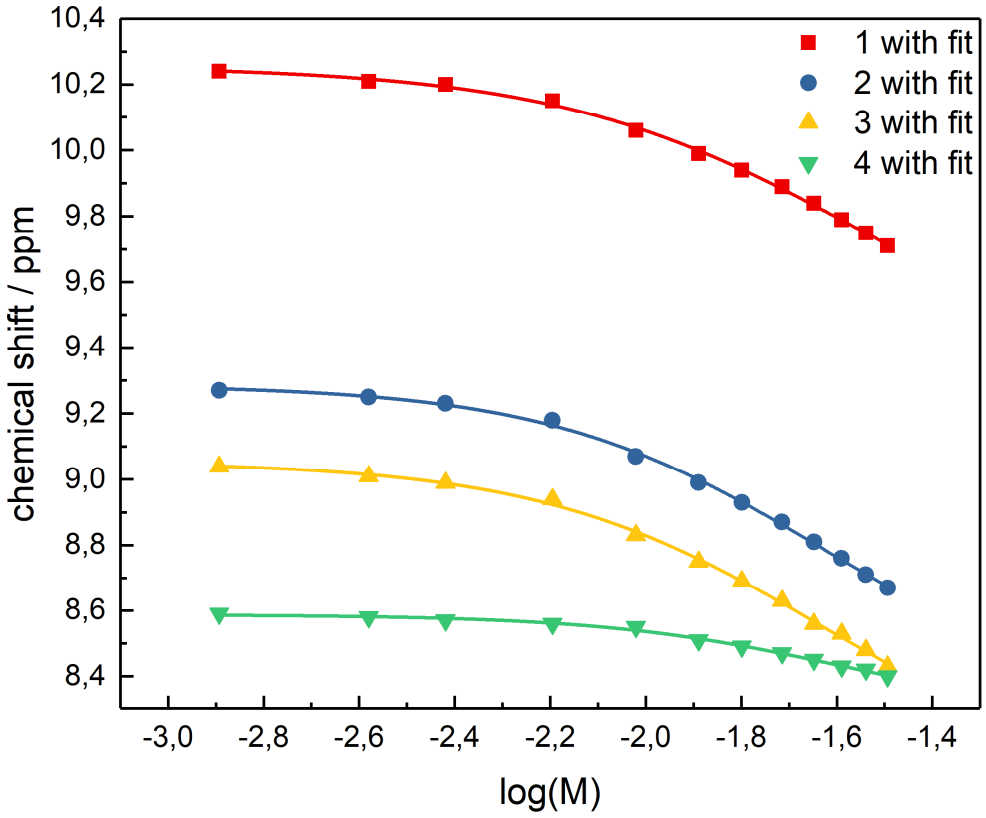

Figure S3.7. Boltzmann fit of the observed chemical shifts versus the logarithm of the investigated concentration range of **Rubiipo**. Correlation $R^2 = 0.9998$.

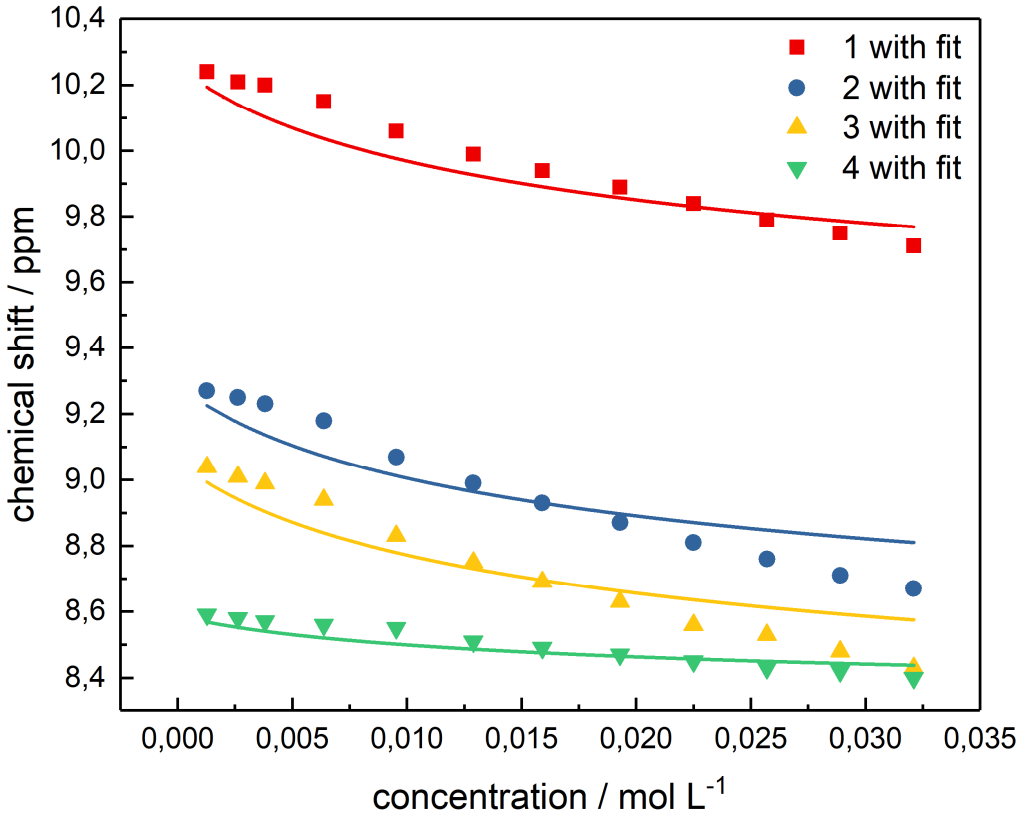

Figure S3.8. Non-linear fit of the observed chemical shifts versus the investigated concentration range of **Rubiipo**. Correlation $R^2 = 0.98747$.

3.2 MS Spectra

ESI mass spectrometry

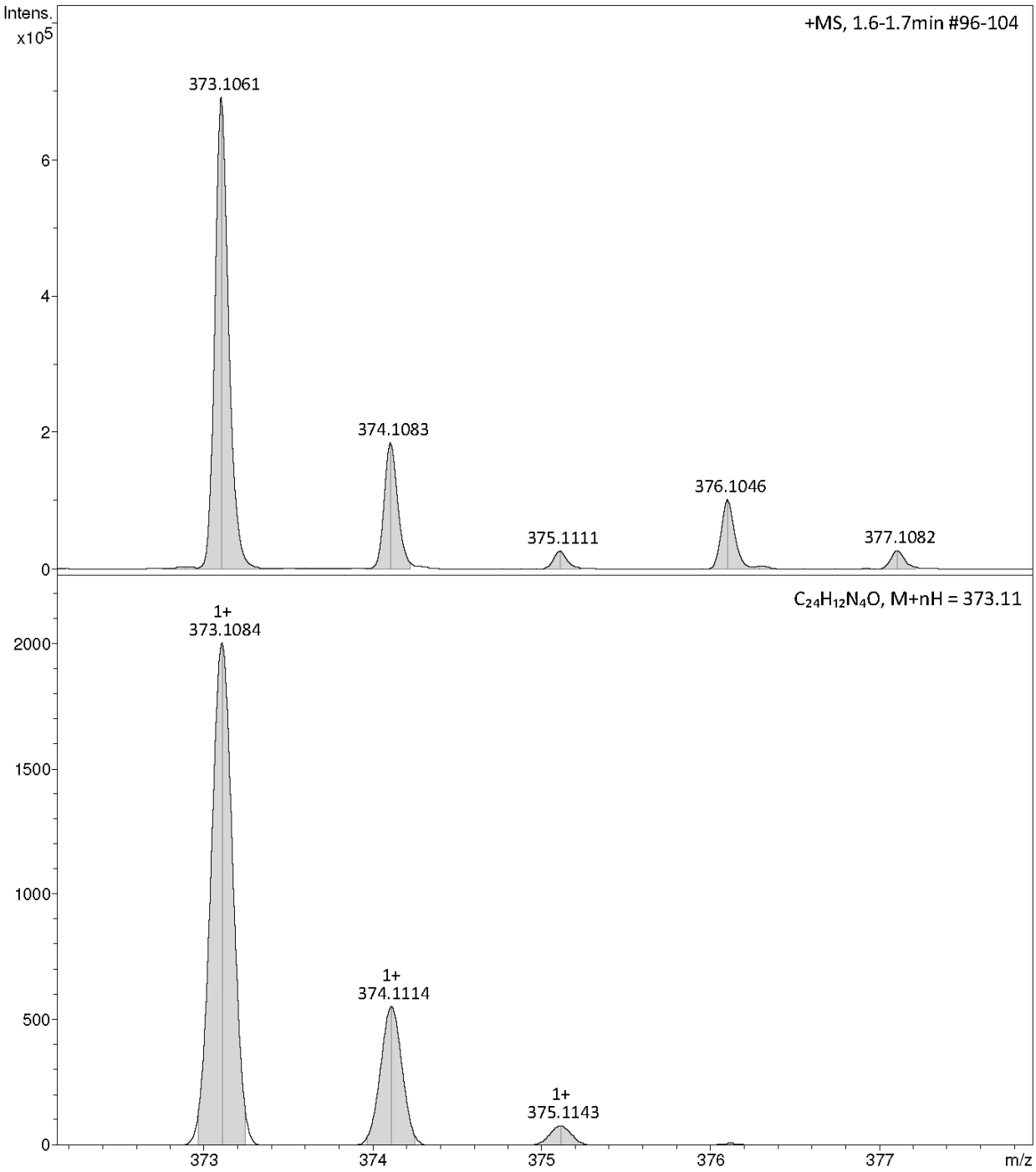

Figure S3.9. Measured (top) and calculated (bottom) ESI-MS spectrum of **biipo**.

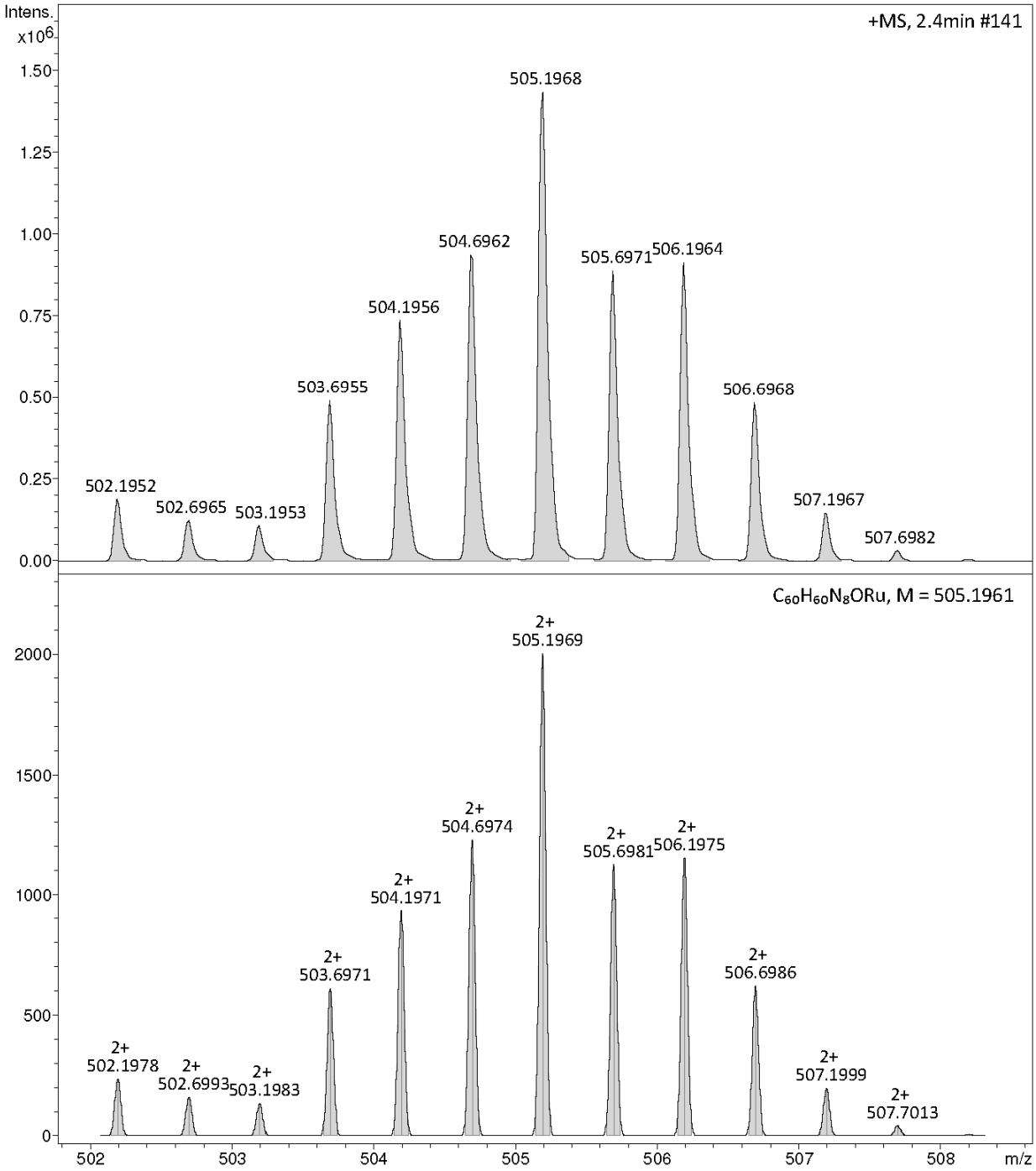

Figure S3.10. Measured (top) and calculated (bottom) high resolution ESI-MS spectrum of **Rubiipo** with matching isotopic pattern.

3.3 X-ray Analysis

Table S3.1. Crystallographic data of **Rubiipo**.

Complex	**Rubiipo**
CCDC number [a]	1993565
Empirical formula	$C_{67.50}\ H_{71.25}\ F_{12}\ N_{11.75}\ O\ P^2\ Ru$
Formula weight	1454.12
Temperature (K)	150(2)
Wavelength (Å)	1.54178
Crystal system, space group	Monoclinic, C2/c
Unit cell dimensions (Å, °) a alpha	 41.9683(5) 90
b beta	24.6149(3) 104.9730(10)
c gamma	15.1304(2) 90
Volume ($Å^3$)	15099.7(3)
Z, Calculated density (Mg m^{-3})	8, 1.279
Absorption coefficient (mm^{-1})	2.738
F(000)	5988
Crystal size (mm)	0.290 x 0.119 x 0.076
Theta range for data collection (°)	3.907 to 76.592
Limiting indices	-52<=h<=52, -30<=k<=30, -17<=l<=19
Reflections collected / unique	69299 / 15715 [R(int) = 0.0431]
Completeness to theta = 67.679	99.8 %
Absorption correction	Gaussian
Max. and min. transmission	1.000 and 0.635
Refinement method	Full-matrix least-squares on F^2
Data / restraints / parameters	15715 / 1190 / 1338
Goodness-of-fit on F^2	1.034
Final R indices [I>2sigma(I)]	R1 = 0.0643, wR2 = 0.1608
R indices (all data)	R1 = 0.0820, wR2 = 0.1689
Largest diff. peak and hole (e.$Å^{-3}$)	1.129 and -0.690

[a] The respective CCDC reference number contains the supplementary crystallographic data for this paper. These data are provided free of charge by the Cambridge Crystallographic Data Centre via www.ccdc.cam.ac.uk/data_request/cif.

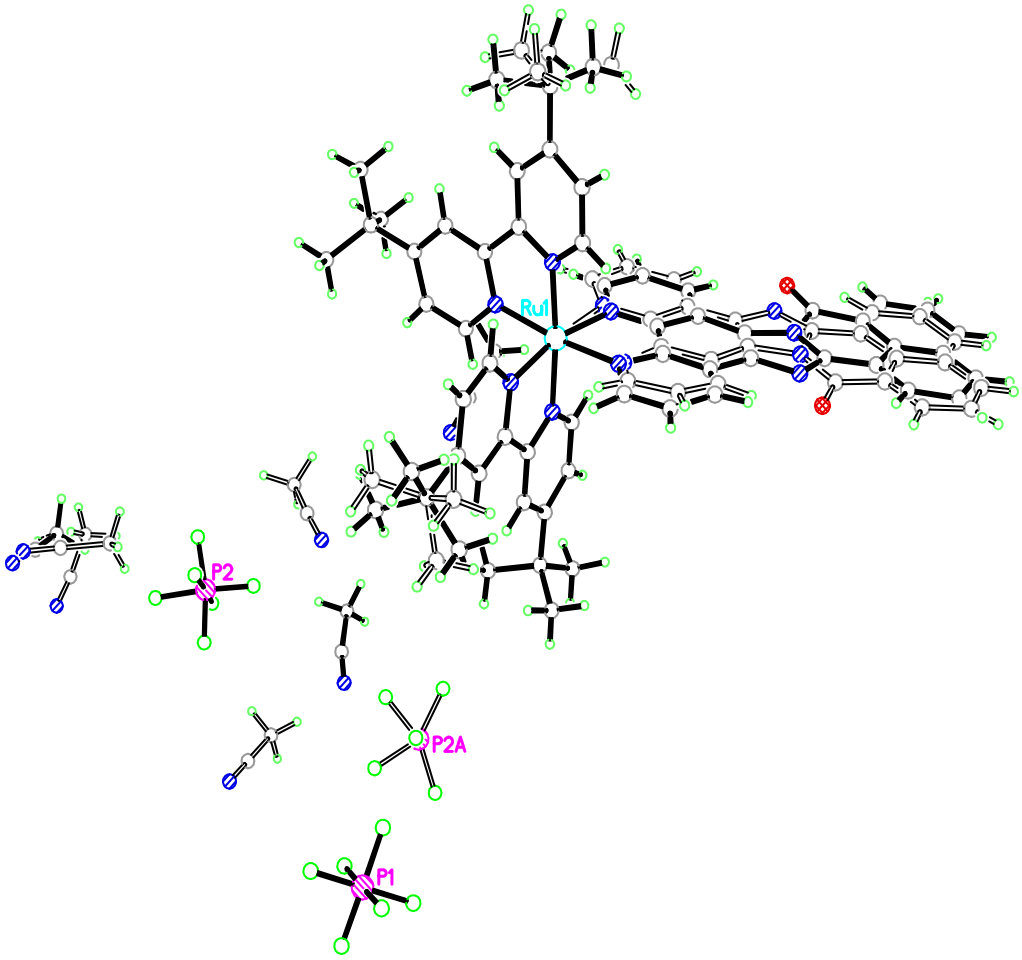

Figure S3.11. Solid-state structure (ORTEP representation) of **Rubiipo**. In comparison to Fig. 3 in the main text the hydrogen atoms, PF_6^- counter anions and solvent molecules are shown. Furthermore, this presentation also depicts the two different coordination modes (isomers) of the asymmetric **biipo** ligand. **Rubiipo** exists as a mixture of two enantiomers, where the biipo ligand shares two different occupancies in the solid state (also cf. Figure S3.12).

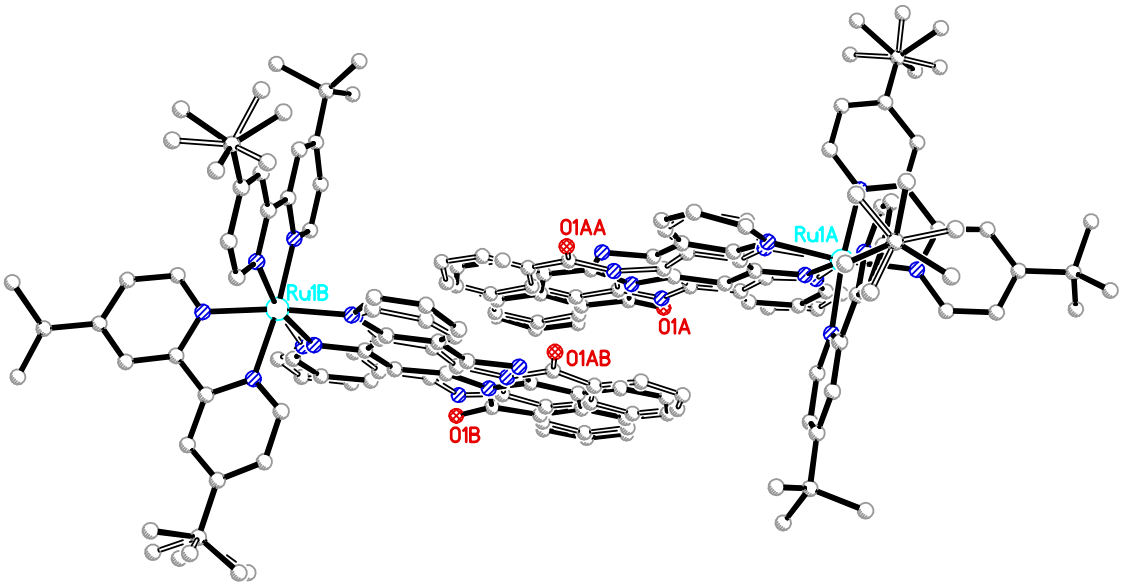

Figure S3.12. ORTEP representation of two neighboring **Rubiipo** molecules showing some π-π interactions between the **biipo** ligand of individual metal complex cations. Hydrogen atoms, PF_6^- counter anions and solvent molecules are omitted for clarity.

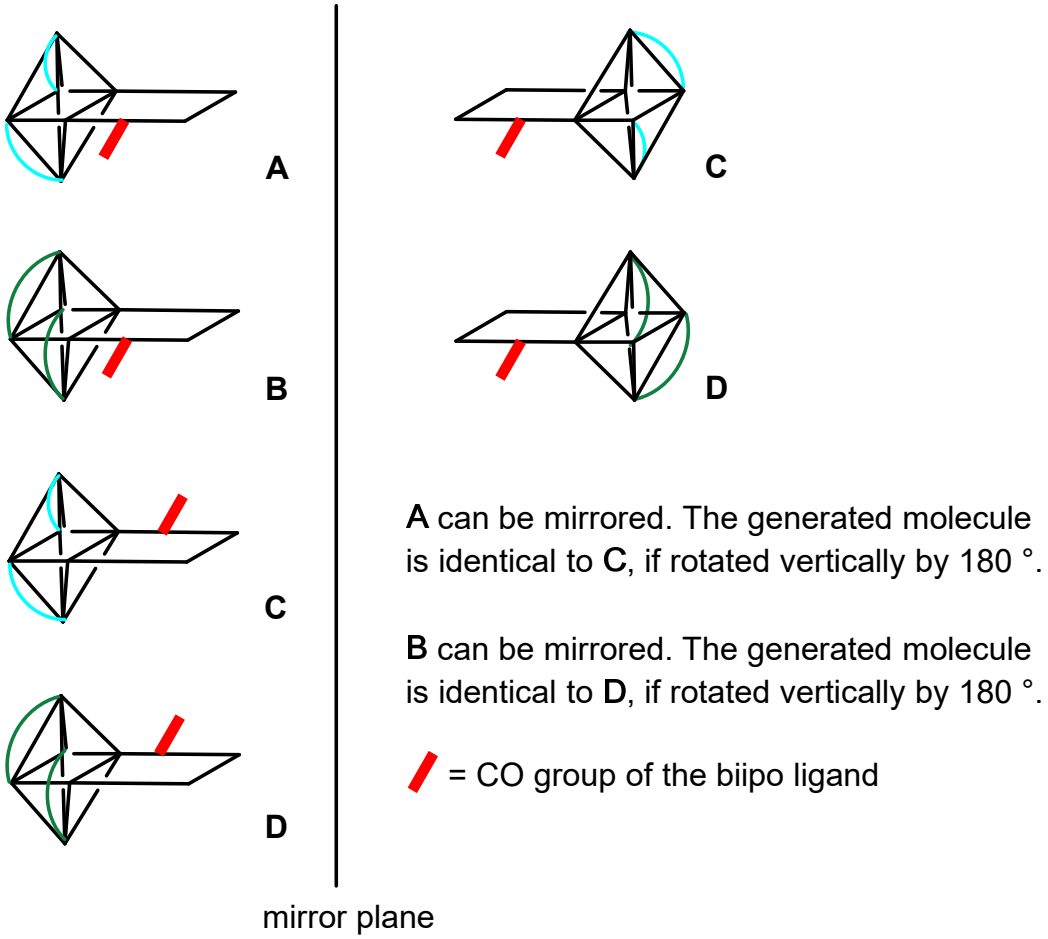

Figure S3.13. Schematic explanation of the stereochemistry of **Rubiipo**. **Rubiipo** does not have different diastereomers, but exists as a mixture of two enantiomers.

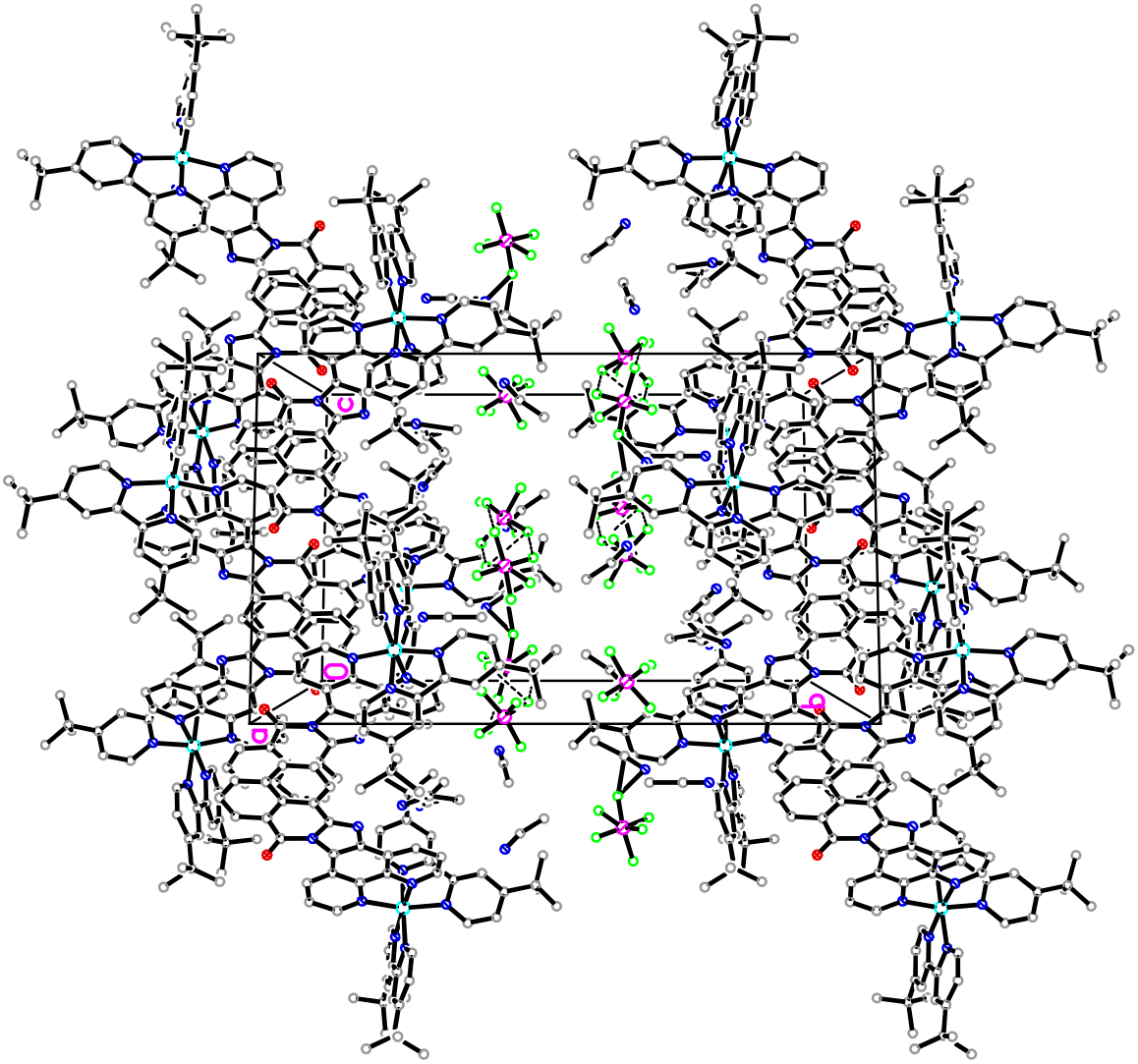

Figure S3.14. ORTEP representation of the unit cell of **Rubiipo** containing 8 Ru complexes, 16 PF_6^- anions and 30 acetonitrile molecules.

3.4 IR Spectra

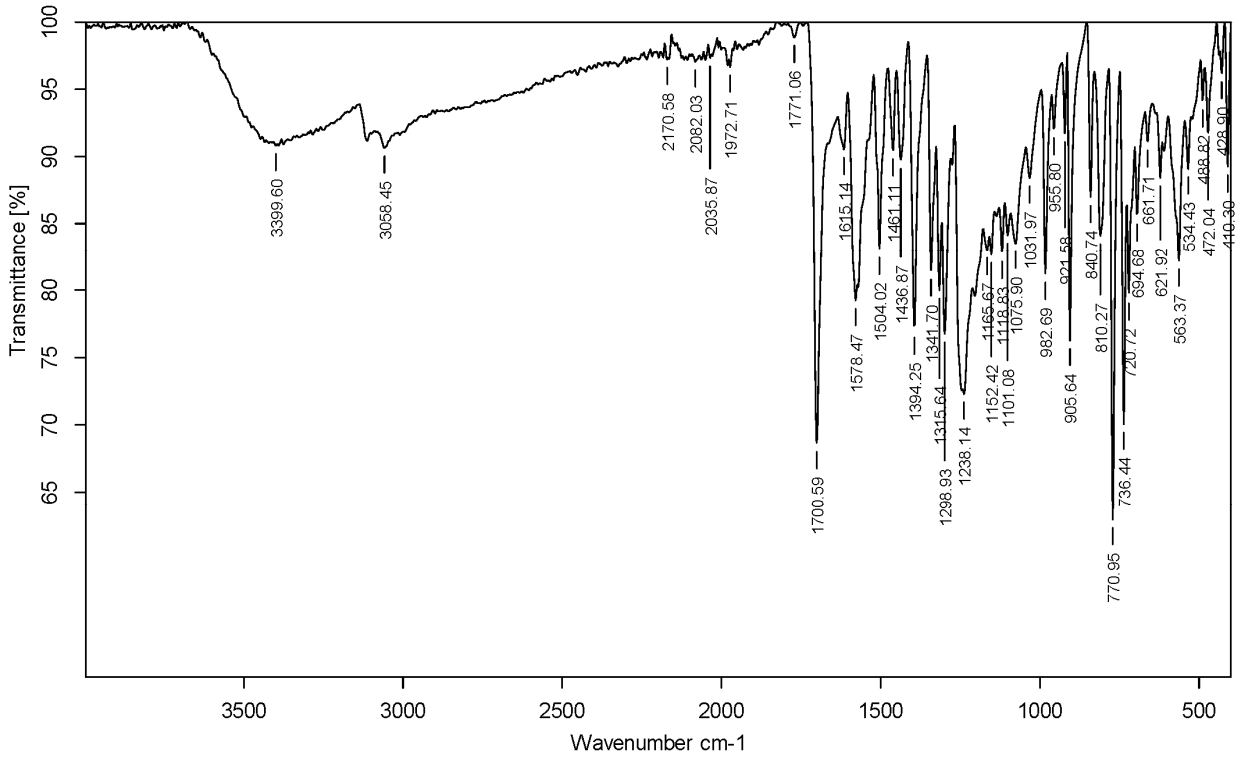

Figure S3.15. Infrared spectrum of **biipo** with a prominent C=O stretching vibration at 1700.6 cm^{-1}.

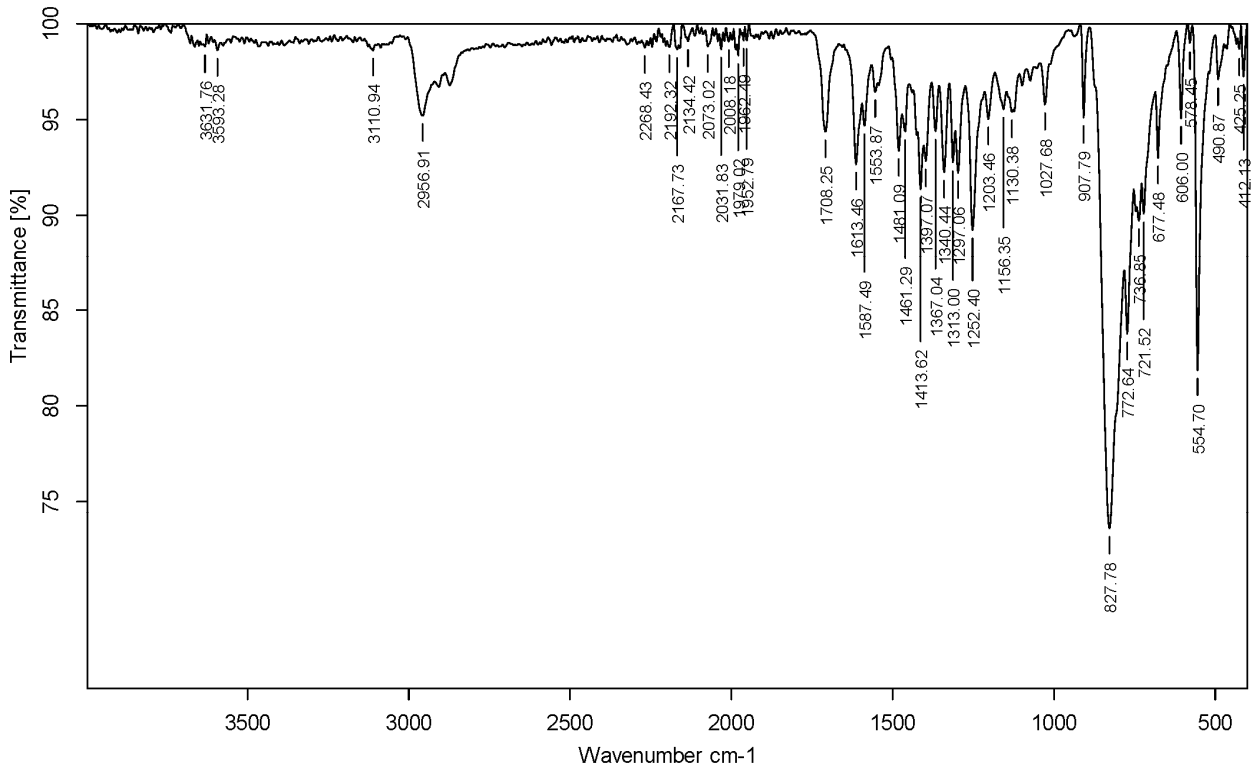

Figure S3.16. Infrared spectrum of **Rubiipo** with a prominent C=O stretching vibration at 1708.3 cm^{-1}.

4 UV/vis and Emission measurements

4.1 Photostability Measurements of biipo and Rubiipo

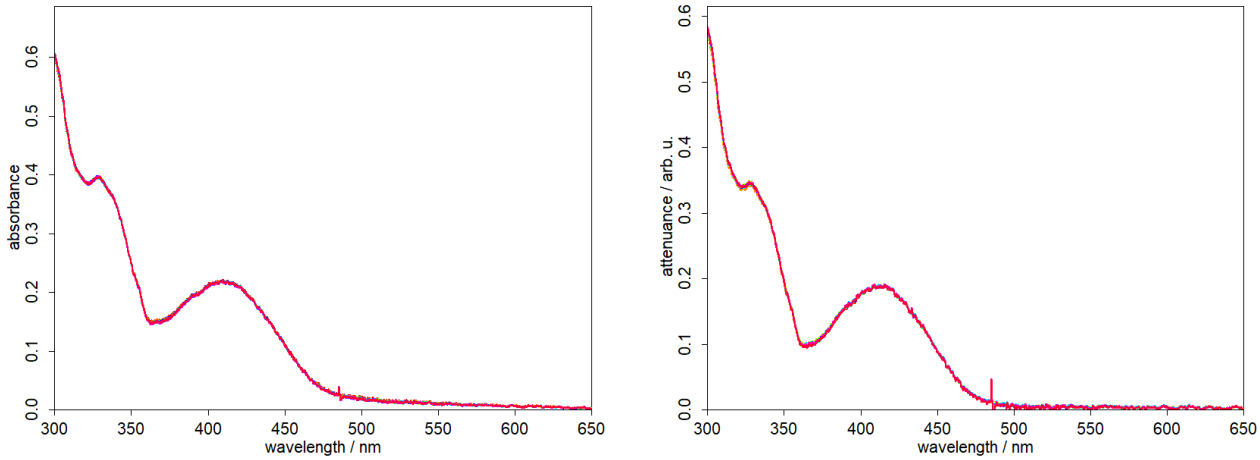

Figure S4.1. UV/vis absorption photostability measurements of **biipo** in oxygen free acetonitrile in the dark (left) and under irradiation (right) with a 150 W Xe arc lamp for 30 min.

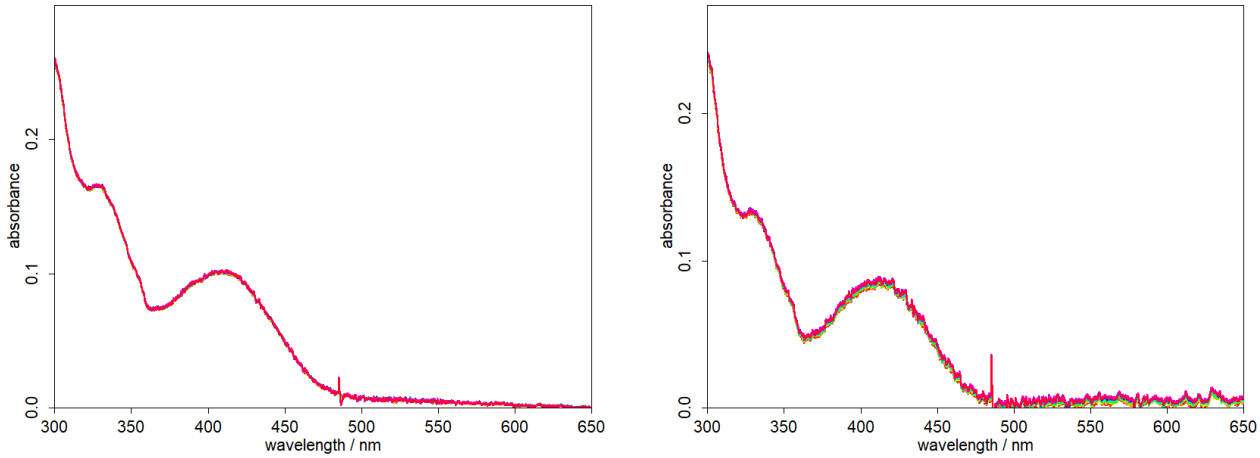

Figure S4.2. UV/vis absorption photostability measurements of **biipo** in aerated acetonitrile in the dark (left) and under irradiation (right) with a 150 W Xe arc lamp for 30 min. The spike at around 490 nm is an artefact caused by the UV/vis spectrometer.

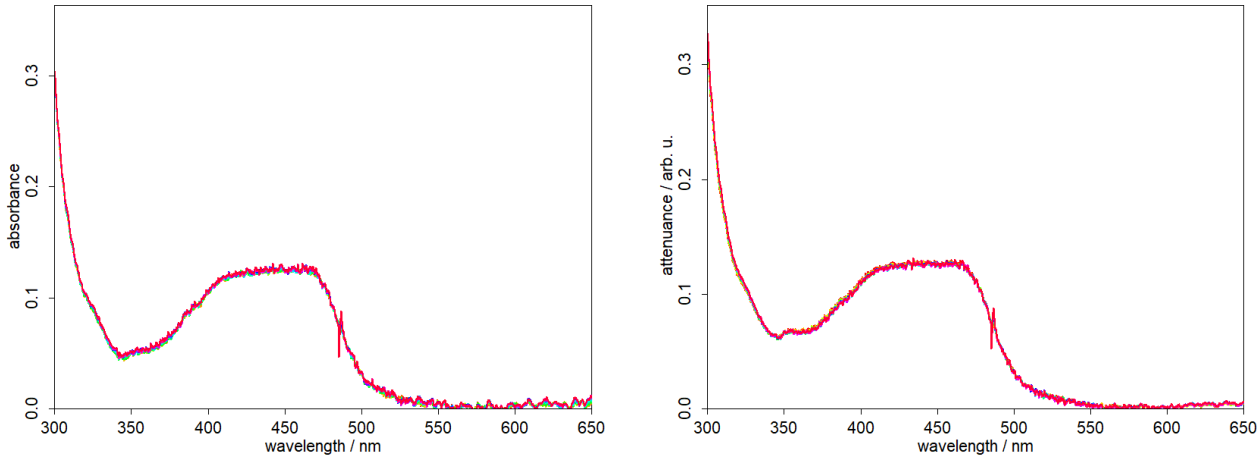

Figure S4.3. UV/vis absorption photostability measurements of **Rubiipo** in oxygen free acetonitrile in the dark (left) and under irradiation (right) with a 150 W Xe arc lamp for 30 min. The spike at around 490 nm is an artefact caused by the UV/vis spectrometer.

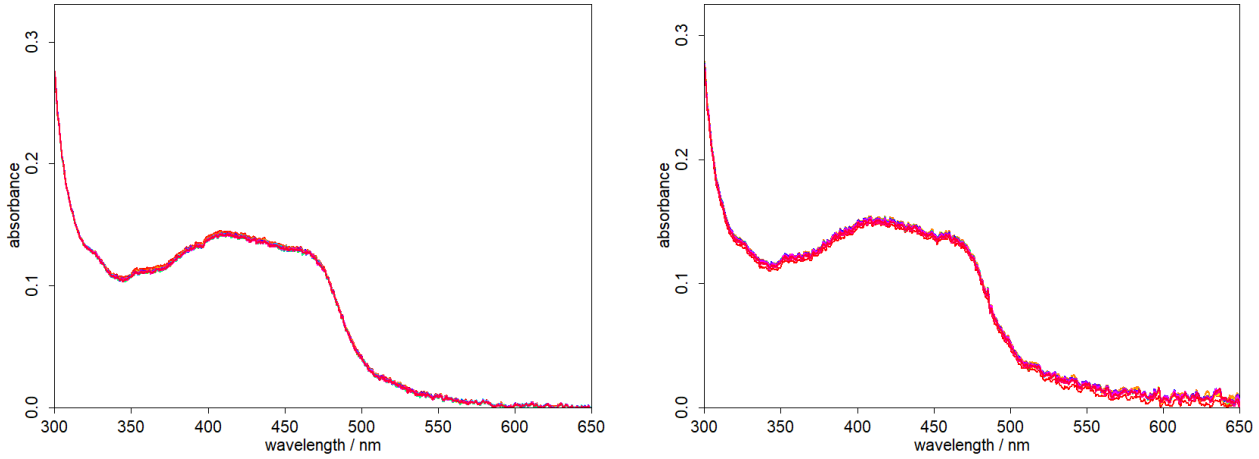

Figure S4.4. UV/vis absorption photostability measurements of **Rubiipo** in aerated acetonitrile in the dark (left) and under irradiation (right) with a 150 W Xe arc lamp for 30 min.

All in all, there is no significant decomposition of **Rubiipo** under these different conditions and **Rubiipo** is quite stable in solution.

4.2 Singlet Oxygen Evolution Experiments

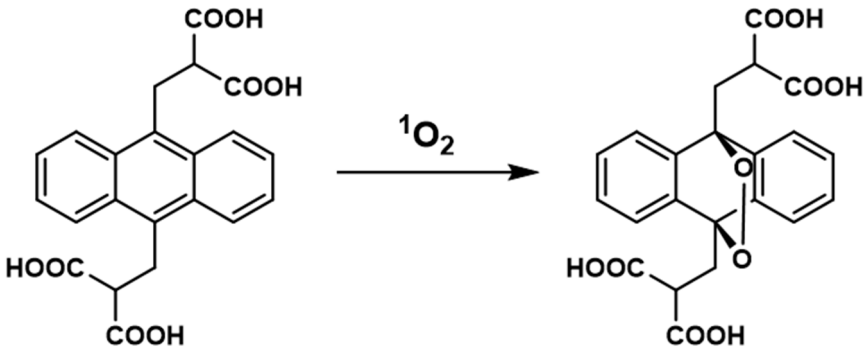

Figure S4.5. Reaction of 9,10-anthracenediyl-bis(methylene)dimalonic acid (ABDA, left) with singlet oxygen ($^1O_2$) forming an endoperoxide of the anthracene derivative.

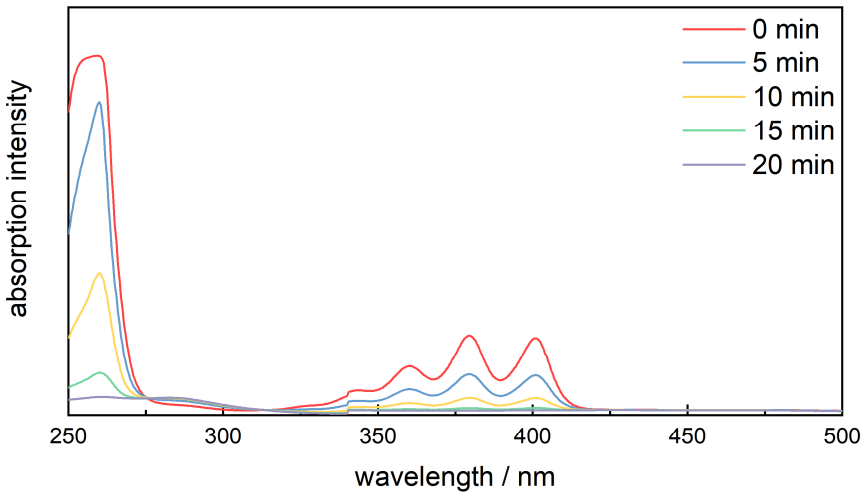

Figure S4.6. Singlet oxygen evolution experiment using **Rubiipo** (1 eq.) and ABDA (50 eq.) in PBS after irradiation with blue light (50 mWcm^{-2}, 470 nm) for different times.

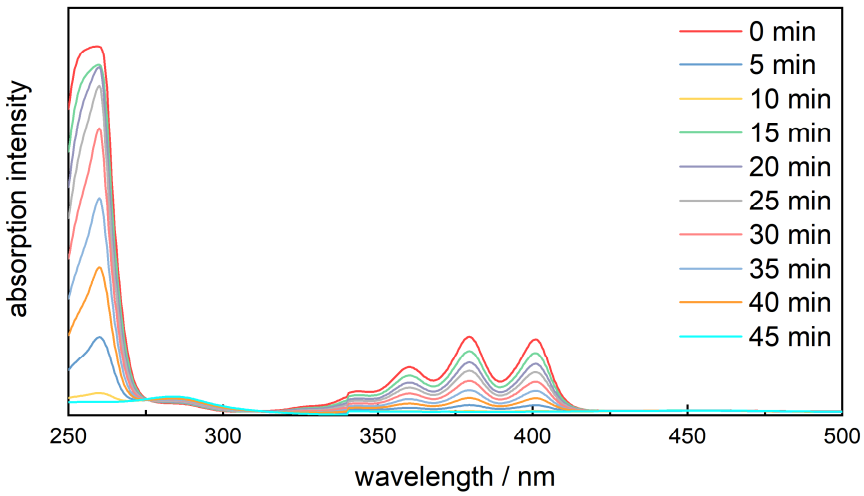

Figure S4.7. Singlet oxygen evolution experiment using **Rubpy** (1 eq.) and ABDA (50 eq.) in PBS after irradiation with blue light (50 mWcm^{-2}, 470 nm) for different times.

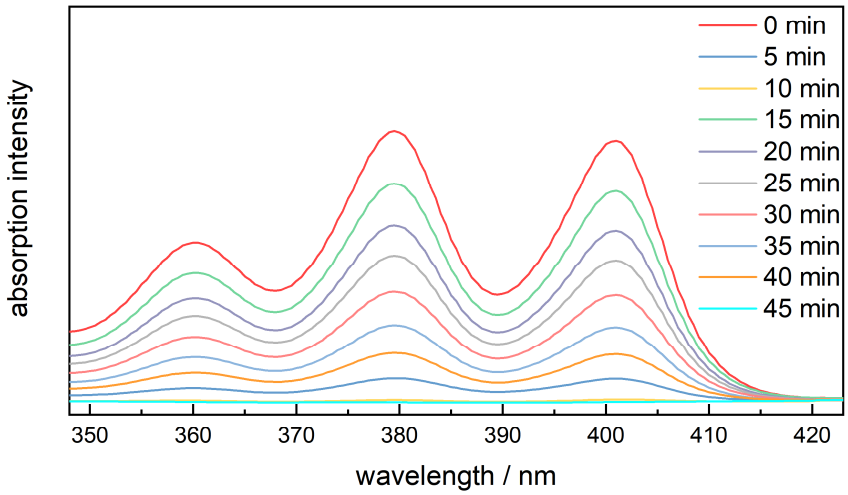

Figure S4.8. Singlet oxygen evolution experiment using **Rubpy** (1 eq.) and ABDA (50 eq.) in PBS after irradiation with blue light (50 mWcm^{-2}, 470 nm) in the range of ABDA absorbance (enlargement of Figure S4.7).

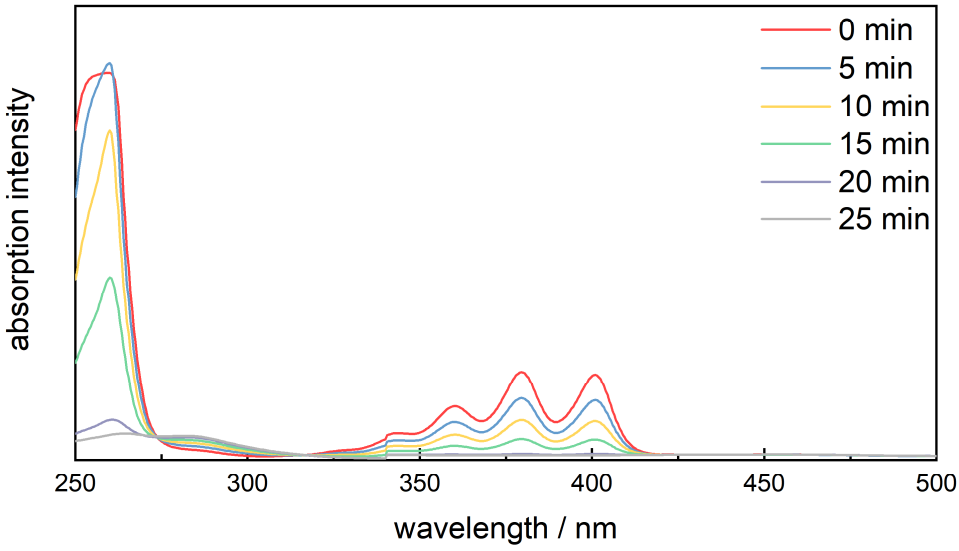

Figure S4.9. Singlet oxygen evolution experiment using **Ruphen** (1 eq.) and ABDA (50 eq.) in PBS after irradiation with blue light (50 mWcm^{-2}, 470 nm) for different times.

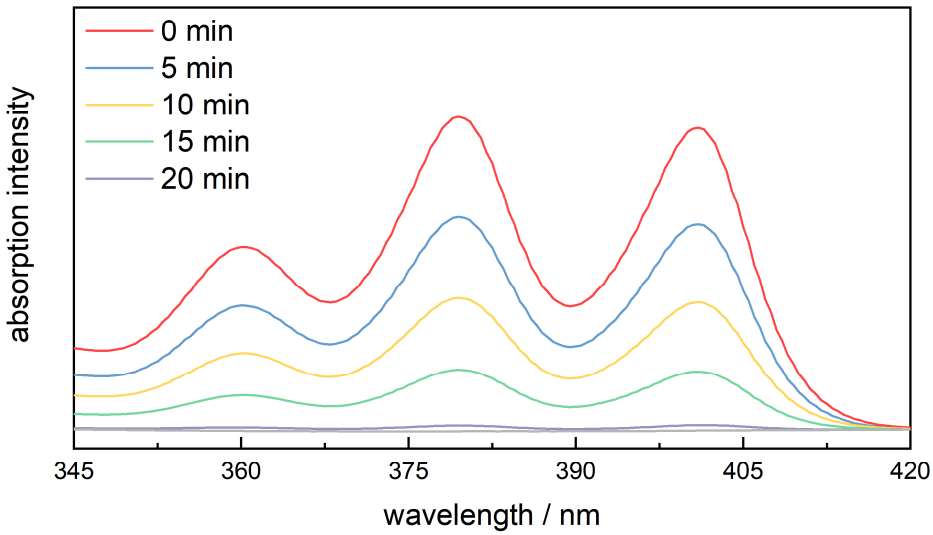

Figure S4.10. Singlet oxygen evolution experiment using **Ruphen** (1 eq.) and ABDA (50 eq.) in PBS after irradiation with blue light (50 mWcm^{-2}, 470 nm) in the range of ABDA absorbance (enlargement of Figure 4.9).

5 Cyclic voltammograms

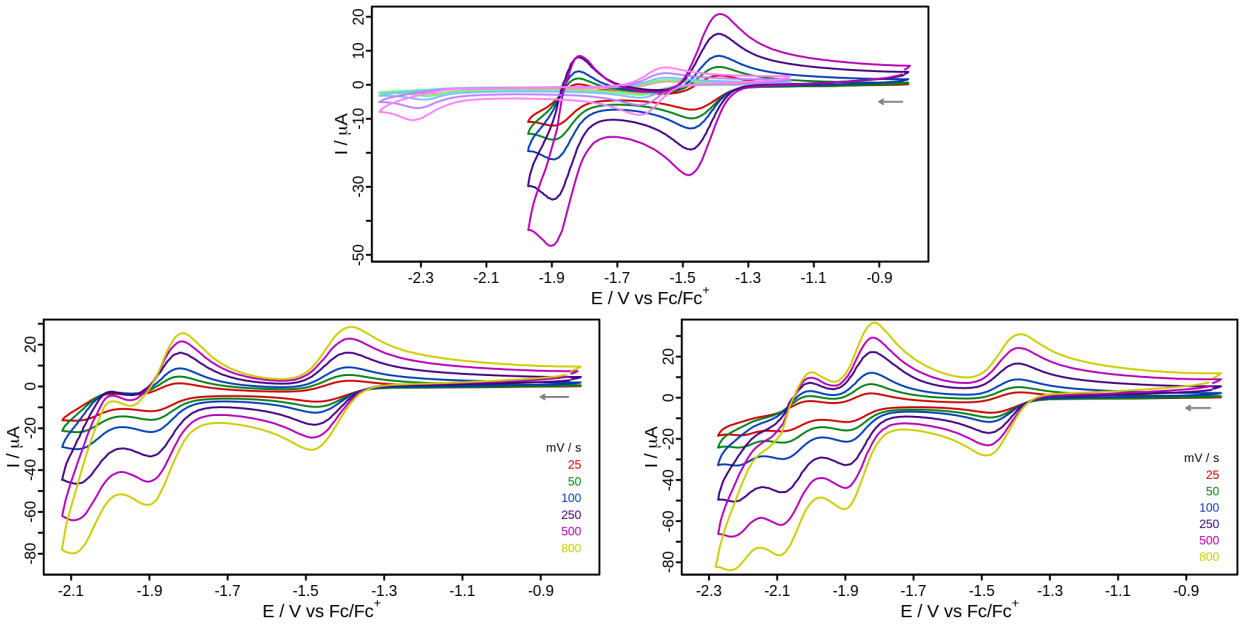

Figure S5.1. Reductive events of the cyclic voltammograms of **biipo** (with light color) and **Rubiipo** (with dark color) in acetonitrile solution referenced vs. the ferrocene/ferricenium (Fc/Fc^+) couple at different scan rates. Conditions: scan rate of 25 mVs^{-1} (red), 50 mVs^{-1} (green), 100 mVs^{-1} (blue), 250 mVs^{-1} (purple), 500 mVs^{-1} (magenta) and 800 mVs^{-1} (yellow), with Bu_4NPF_6 (0.1 M) as supporting electrolyte. The arrow illustrates the initial scan direction. Top: First two reduction events. Bottom left: Three reduction events. Bottom right: All for reduction events at once.

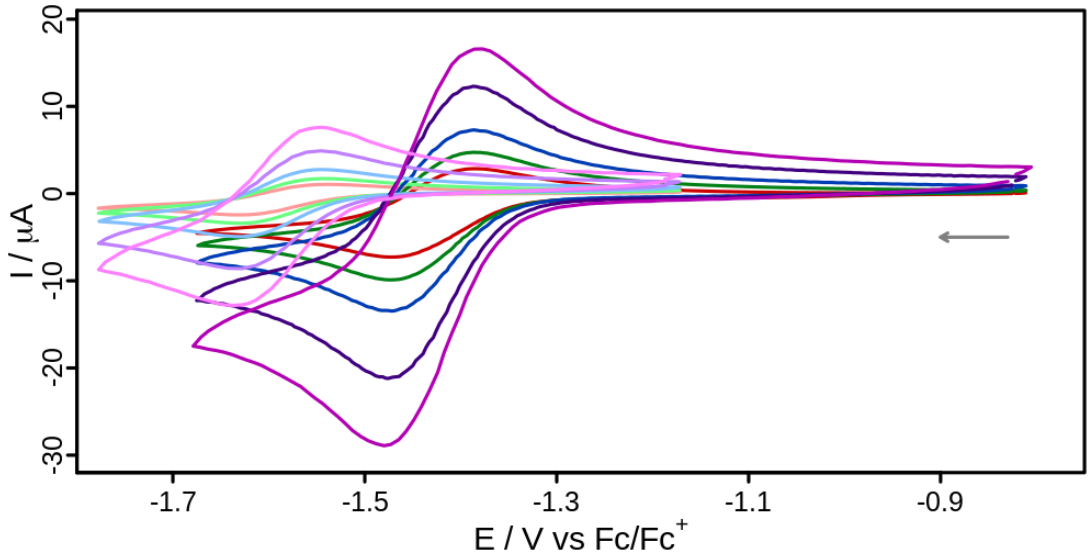

Figure S5.2. Cyclic voltammograms of the first reduction event of **biipo** (with light color) and **Rubiipo** (with dark color) in acetonitrile solution referenced *vs*. the ferrocene/ferricenium (Fc/Fc^+) couple at different scan rates. Conditions: scan rate of 25 mVs^{-1} (red), 50 mVs^{-1} (green), 100 mVs^{-1} (blue), 250 mVs^{-1} (purple) and 500 mVs^{-1} (violet).

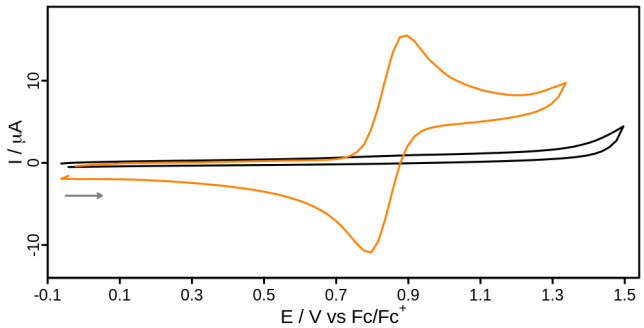

Figure S5.3. Oxidative part of the cyclic voltammograms of **biipo** (black, < 1 mM due to lower solubility in acetonitrile) and **Rubiipo** (orange, 1mM) in acetonitrile solution referenced vs. the ferrocene/ferricenium (Fc/Fc^+) couple. Conditions: scan rate of 100 mVs^{-1}, Bu_4NPF_6 (0.1 M) as supporting electrolyte. The arrow illustrates the initial scan direction.

6 Emission Lifetime Measurements

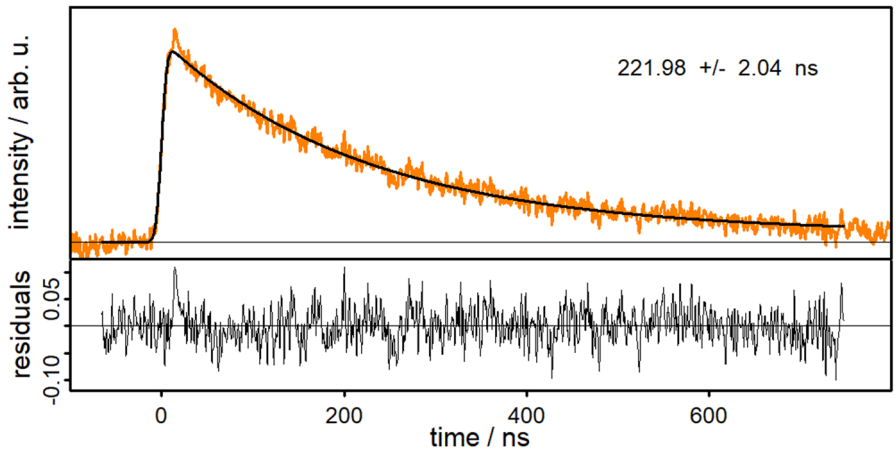

Figure S6.1. Excited-state lifetimes of **Rubiipo** (orange) in aerated acetonitrile solution. The optical density is 0.1 at 355 nm. The experimental results are monoexponentially fitted (black) and the lifetime is 222 ns.

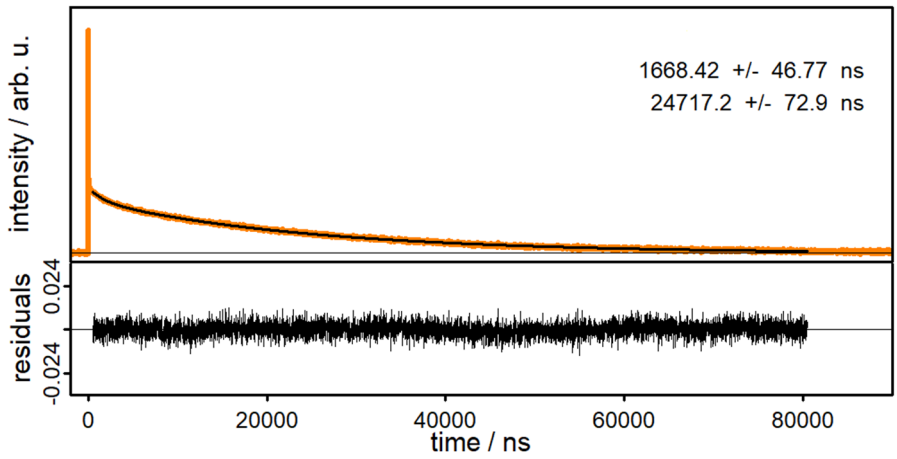

Figure S6.2. Excited-state lifetimes of **Rubiipo** (orange) in oxygen free acetonitrile solution. The optical density is 0.1 at 355nm. The experimental results are bi-exponentially fitted (black) and the lifetimes are 1668 ns and 24717 ns.

7 Transient Absorption Measurements

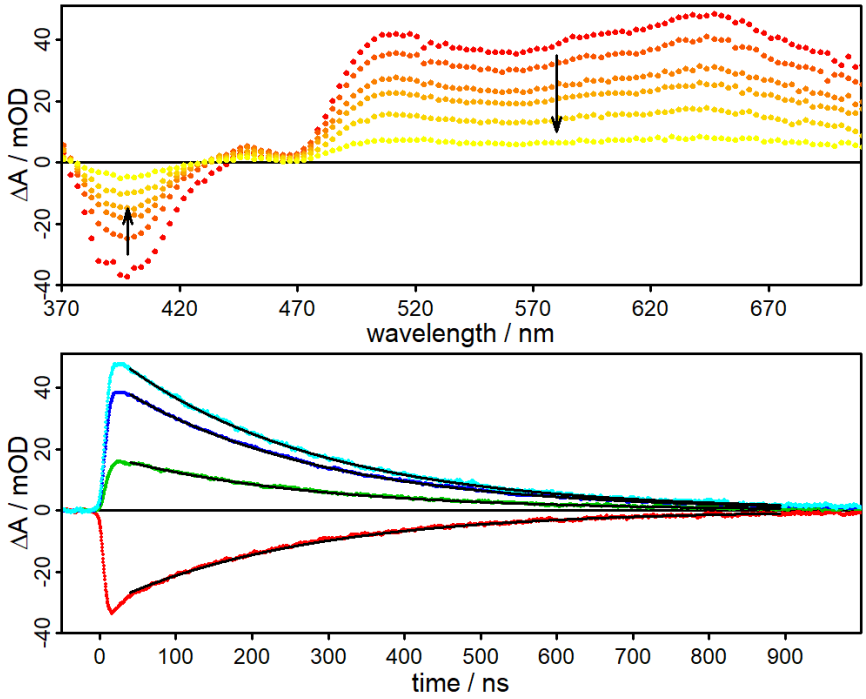

Figure 7.1. Transient absorption spectra (top) and respective kinetics (bottom) of **Rubiipo** in acetonitrile excited at 355 nm under aerated conditions.
Top: Spectra from 20 (red) to 500 ns (yellow). Bottom: Kinetics at 390 (red), 480 (green), 500 (blue) and 650 nm (light blue), the black line belongs to the fits with a time constant of 261 ns.

8 Calculated Ground State Structures of biipo and Rubiipo

The optimized ground state structure of biipo and Rubiipo were calculated based on density functional theory (DFT) with a conductor-like polarizable continuum solvent correction based on acetonitrile (Figure S8.1, Table S8.1). The structures were optimized at the BP86/def2-TZVP level of theory.

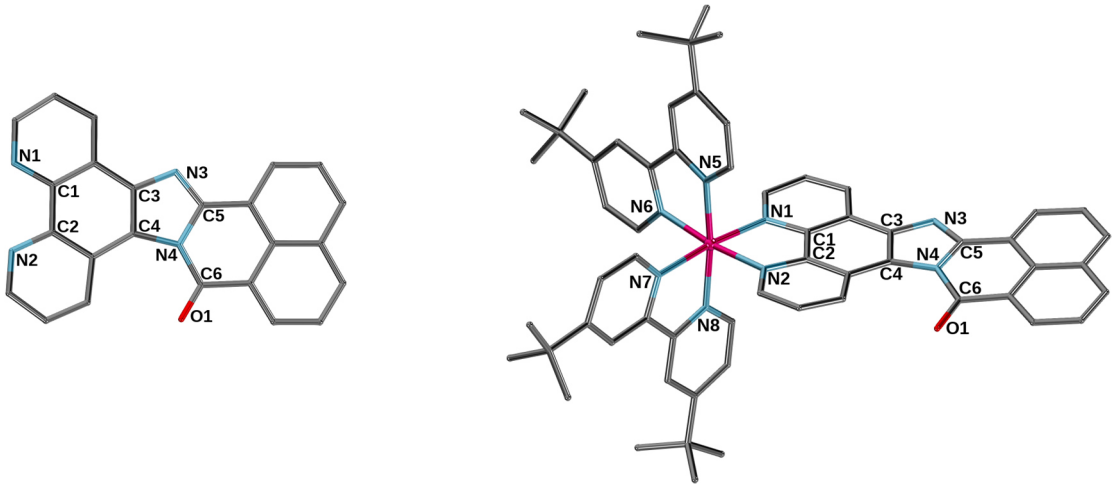

Figure S8.1. Calculated ground state (S_0) structure of **biipo** (left) and **Rubiipo** (right). Hydrogen atoms are omitted for clarity.

Table S8.1. Selected bond lengths (pm) and angles (°) of the calculated ground state (S_0) structure BP86/def2-TZVP) of **C1** in acetonitrile. For atom labeling see structures in Figure S8.1.

	S_0 of **Rubiipo**		S_0 of **biipo**	S_0 of **Rubiipo**		S_0 of **biipo**	S_0 of **Rubiipo**
Ru-N1	206.1	N1-N2	271.8	263.2	N3-C5	131.6	132.0
Ru-N2	207.1	N3-N4	226.7	226.7	N4-C5	141.3	141.0
Ru-N5	206.7	C1-C2	146.5	143.3	N4-C6	142.4	142.8
Ru-N6	206.4	C3-C4	140.0	140.4	C6-O1	122.6	122.6
Ru-N7	206.6	C3-N3	137.5	137.3	C3-N3-C5	105.6	105.4
Ru-N8	206.5	C4-N4	142.5	141.2	C4-N4-C5	105.9	106.1
N1-Ru-N2	79.1						
N5-Ru-N6	78.4						
N7-Ru-N8	78.5						

The calculated Ru-N bond lengths of about 206.5 - 207.1 pm and the N-Ru-N angles with approx. 78.7° have typical values for ruthenium complexes with a 2,2'-bipyridine or 1,10-phenanthroline ligand.[21]
It is obvious that the coordination of the ligand to the ruthenium center leads to a shortening of the N1-N2 and the C1-C2 distance. Thus, only the phenanthroline part of the **biipo** ligand is affected and the naphthaloylenebenzene unit not.

[21] C. Kuhnt, S. Tschierlei, M. Karnahl, S. Rau, B. Dietzek, M. Schmitt, J. Popp, *J. Raman Spectrosc.* **2010**, *41*, 922–932.

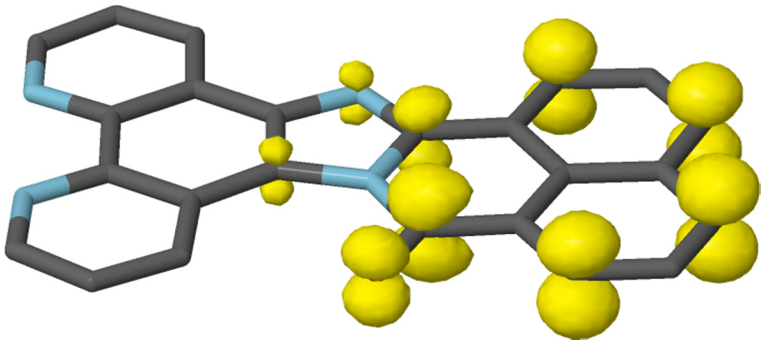

Figure S8.2. Visualization of the spin density of the singly reduced **biipo** ligand showing that the first reduction is located at the naphthaloylenebenzenimidazole moiety. Hydrogen atoms are omitted for clarity.

9 TD-DFT Calculations of the Absorption Spectra of biipo and Rubiipo

Table S9.1. Calculated excitation energies and transition moments of **biipo** at full TD-DFT level (B3LYP-D3(BJ)/def2-TZVP). Only excitations with an oscillator strength > 0.01 and corresponding orbital contributions with $|coeff.|^2 \geq 0.2$ are listed. Compare with the differential densities in Figure S9.1 and the orbital pictures in Figure S9.2.

Exc.	Excitation energy		Oscillator strength	Dominant contributions			Transitions
#	cm^{-1}	Nm	length representation	occ. orbital	virt. orbital	$\|coeff.\|^2$ *100	
1	20826.7	480.2	0.181251651	HOMO	LUMO	0.916682	$\pi_{phen, im, naph} \rightarrow \pi_{naph}$
2	26545.2	376.7	0.071583991	HOMO-1	LUMO	0.752488	$\pi_{phen} \rightarrow \pi_{naph}$
3	28466.0	351.3	0.116565967	HOMO	LUMO+1	0.739384	$\pi_{phen, im, naph} \rightarrow \pi_{phen}$
5	30670.4	326.0	0.040360250	HOMO-2	LUMO	0.767241	$\pi_{phen, naph} \rightarrow \pi_{naph}$
6	31609.8	316.4	0.059904964	HOMO-4	LUMO	0.664023	$\pi_{naph} \rightarrow \pi_{naph}$
7	31930.4	313.2	0.024764925	HOMO	LUMO+2	0.686247	$\pi_{phen, im, naph} \rightarrow \pi_{phen}$
10	33722.0	296.5	0.516928675	HOMO	LUMO+3	0.808414	$\pi_{phen, im, naph} \rightarrow \pi_{phen, im, naph}$
12	35117.3	284.8	0.045074337	HOMO-1	LUMO+1	0.481540	$\pi_{phen} \rightarrow \pi_{phen}$
14	36285.6	275.6	0.010046742	HOMO	LUMO+4	0.397158	$\pi_{phen, im, naph} \rightarrow \pi_{naph}$
15	37680.0	265.4	0.120813143	HOMO-1	LUMO+2	0.270434	$\pi_{phen} \rightarrow \pi_{phen}$
				HOMO	LUMO+4	0.210825	$\pi_{phen, im, naph} \rightarrow \pi_{naph}$
17	37000.7	270.3	0.041345563	HOMO-9	LUMO	0.260268	$\pi_{phen, im} \rightarrow \pi_{naph}$
				HOMO-10	LUMO	0.239756	$\pi_{phen, im} \rightarrow \pi_{naph}$

phen = phenanthroline part
naph = naphthaloylenebenzene part
im = imidazole part

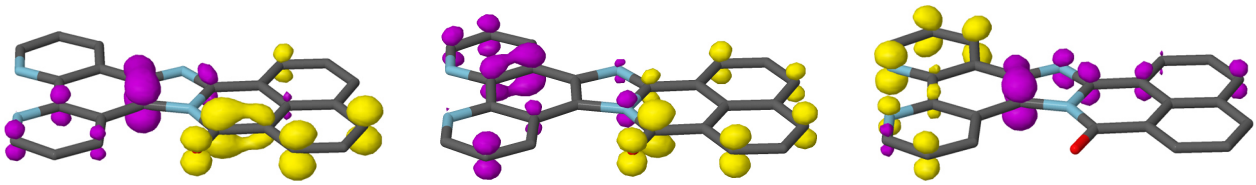

transition 1 transition 2 transition 3

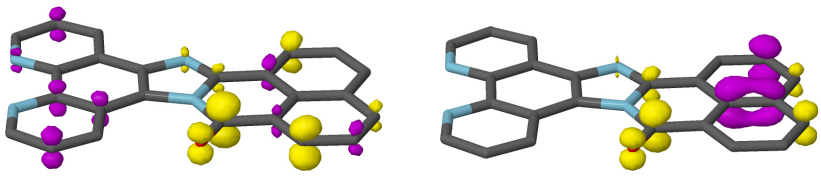

transition 5 transition 6

Figure S9.1. Differential density plots of **biipo** between the ground state and several excited states. The positive contributions are marked in yellow and the negative values in magenta.

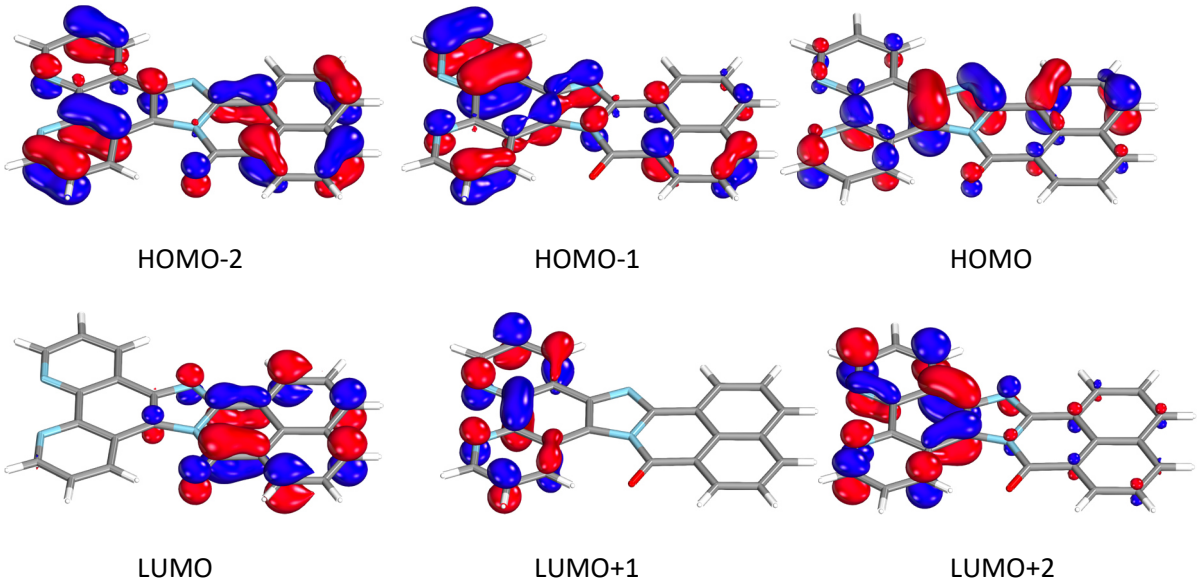

Figure S9.2. Presentation of the orbitals of ligand **biipo** at B3LYP-D3(BJ)/def2-TZVP level of theory.

Table S9.2. Calculated excitation energies and transition moments of **Rubiipo** at full TD-DFT level (B3LYP-D3(BJ)/def2-TZVP). Only excitations with an oscillator strength > 0.01 and corresponding orbital contributions with $|coeff.|^2 \geq 0.2$ are listed. Compare with the differential densities in Figure S9.3 and the orbital pictures in Figure S9.4. The π-π* transitions are marked in grey.

Excitation	**Excitation energy**		**Oscillator strength**	**Dominant contributions**			**Transitions**
#	cm^{-1}	Nm	length representation	occ. orbital	virt. orbital	$\|coeff.\|^2$ *100	
3	20410.5	489.9	0.010056265	0.710481	HOMO	LUMO+2	$d_{Ru} \rightarrow \pi_{tbbpy}$
5	18752.5	533.3	0.029476656	0.337449	HOMO-2	LUMO	$d_{Ru} \rightarrow \pi_{naph}$
				0.430700	HOMO-1	LUMO	$d_{Ru} \rightarrow \pi_{naph}$
8	21872.4	457.2	0.049650709	0.201875	HOMO-2	LUMO+2	$d_{Ru} \rightarrow \pi_{tbbpy}$
				0.303160	HOMO-1	LUMO+1	$d_{Ru} \rightarrow \pi_{phen}$
				0.215474	HOMO-1	LUMO+2	$d_{Ru} \rightarrow \pi_{tbbpy}$
9	22123.4	452.0	0.037613399	0.218069	HOMO-2	LUMO+2	$d_{Ru} \rightarrow \pi_{tbbpy}$
				0.297073	HOMO-1	LUMO+2	$d_{Ru} \rightarrow \pi_{tbbpy}$
10	22918.7	436.3	0.231646806	0.241667	HOMO-2	LUMO+2	$d_{Ru} \rightarrow \pi_{tbbpy}$
				0.254627	HOMO-1	LUMO+1	$d_{Ru} \rightarrow \pi_{phen}$
11	23108.9	432.7	0.125391590	0.329938	HOMO-2	LUMO+3	$d_{Ru} \rightarrow \pi_{tbbpy}$
				0.265545	HOMO-1	LUMO+3	$d_{Ru} \rightarrow \pi_{tbbpy}$
12	23962.4	417.3	0.309713217	0.588237	HOMO-3	LUMO	$d_{Ru}, \pi_{phen,\ im} \rightarrow \pi_{naph}$
15	26210.2	381.5	0.040694242	0.202157	HOMO-1	LUMO+4	$d_{Ru} \rightarrow \pi_{phen,\ im}$
				0.255281	HOMO	LUMO+4	$d_{Ru} \rightarrow \pi_{phen,\ im}$
16	26346.0	379.6	0.023675282	0.442266	HOMO-3	LUMO+1	$d_{Ru}, \pi_{im,\ naph} \rightarrow \pi_{phen}$
				0.269413	HOMO-1	LUMO+4	$d_{Ru} \rightarrow \pi_{phen,im}$
17	26724.2	374.2	0.028526870	0.726538	HOMO	LUMO+5	$d_{Ru} \rightarrow \pi_{tbbpy}$
18	26949.6	371.1	0.048299936	0.328543	HOMO-3	LUMO+1	$d_{Ru}, \pi_{im,\ naph} \rightarrow \pi_{phen}$
19	28089.4	356.0	0.018262016	0.694115	HOMO-1	LUMO+5	$d_{Ru} \rightarrow \pi_{tbbpy}$
23	29062.7	344.1	0.061507355	0.367422	HOMO-4	LUMO	$\pi_{phen,\ im,\ naph} \rightarrow \pi_{naph}$
				0.316209	HOMO-3	LUMO+4	$d_{Ru}, \pi_{im,\ naph} \rightarrow \pi_{phen,\ im}$
24	29173.0	342.8	0.010101348	0.238214	HOMO	LUMO+8	$d_{Ru} \rightarrow \pi_{tbbpy}$
25	27743.7	360.4	0.015889563	0.580577	HOMO-3	LUMO+3	$d_{Ru}, \pi_{im,\ naph} \rightarrow \pi_{tbbpy}$
28	30158.1	331.6	0.020101218	0.500143	HOMO-1	LUMO+7	$d_{Ru} \rightarrow \pi_{tbbpy}$
30	30747.1	325.2	0.062081169	0.408743	HOMO-3	LUMO+4	$d_{Ru}, \pi_{im,\ naph} \rightarrow \pi_{phen,\ im}$
31	30760.4	325.1	0.063260763	0.291836	HOMO	LUMO+9	$d_{Ru} \rightarrow \pi_{tbbpy}$
32	30955.0	323.0	0.034839567	0.352999	HOMO-1	LUMO+6	$d_{Ru} \rightarrow \pi_{phen,im,naph}$
33	30911.2	323.5	0.022829941	0.348574	HOMO-1	LUMO+9	$d_{Ru} \rightarrow \pi_{tbbpy}$
35	31425.9	318.2	0.052874407	0.219393	HOMO-7	LUMO	$\pi_{phen,\ im,\ naph} \rightarrow \pi_{naph}$
37	28068.7	356.3	0.011186982	0.877151	HOMO-5	LUMO	$\pi_{tbbpy} \rightarrow \pi_{naph}$
38	30320.0	329.8	0.027864737	0.604042	HOMO-6	LUMO	$\pi_{tbbpy} \rightarrow \pi_{naph}$
39	30992.7	322.7	0.054793592	0.293811	HOMO-8	LUMO	$\pi_{phen,\ naph} \rightarrow \pi_{naph}$
				0.325736	HOMO-6	LUMO	$\pi_{tbbpy} \rightarrow \pi_{naph}$

tbbpy = 4,4'-*tert*.-butyl-2,2'-bipyridine ligand

phen = 1,10-phenanthroline part

naph = naphthaloylenebenzene part

im = imidazole part

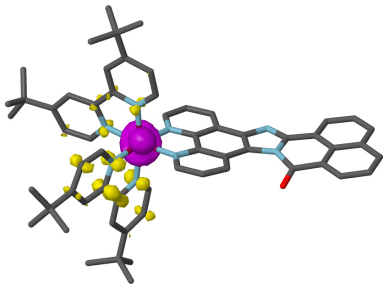

transition 3

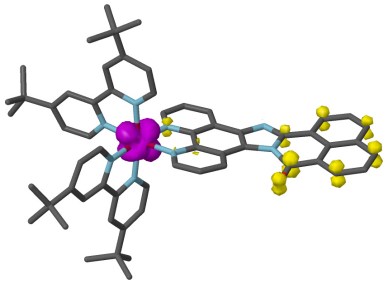

transition 5

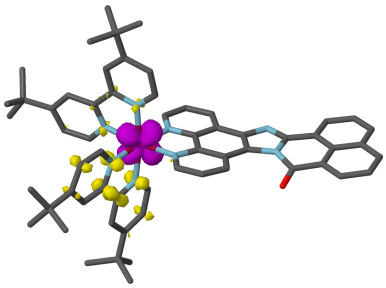

transition 8

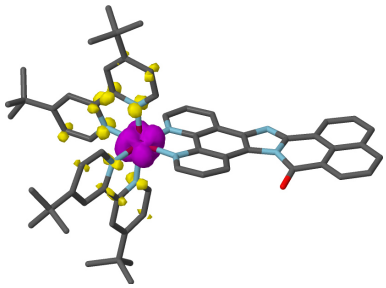

transition 9

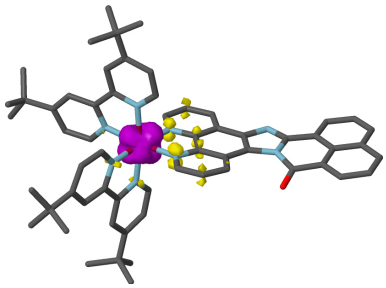

transition 10

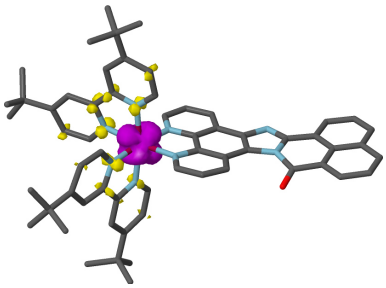

transition 11

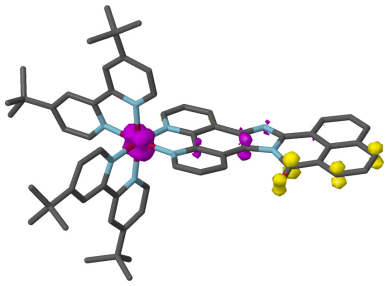

transition 12

Figure S9.3. Differential density plots of **Rubiipo** between the ground state and several excited states. The positive contributions are marked in yellow and the negative values in magenta. Transition 5 is located at the lowest energy, compare with Table 9.2. The first π-π* transition occurs at transition 12.

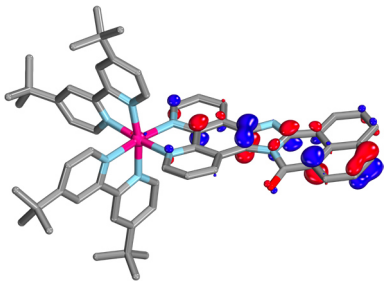

HOMO-4

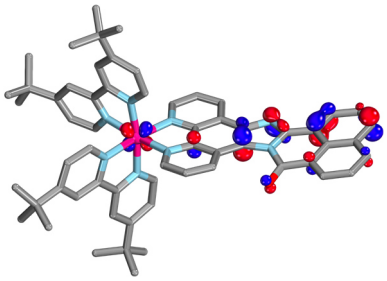

HOMO-3

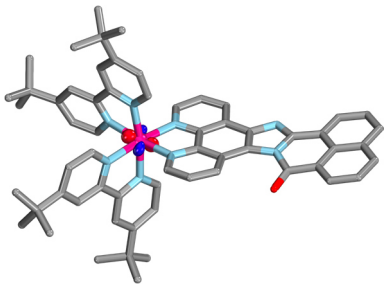

HOMO-2

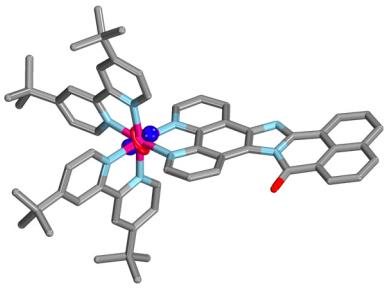

HOMO-1

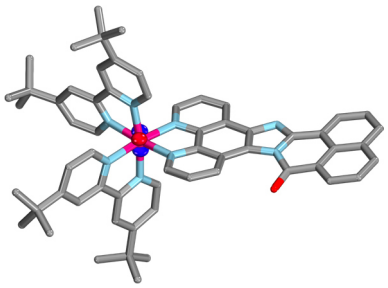

HOMO

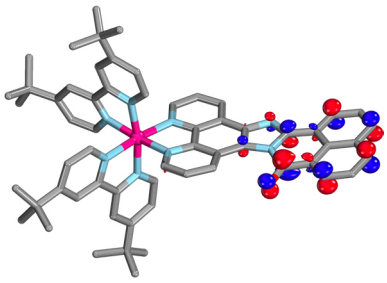

LUMO

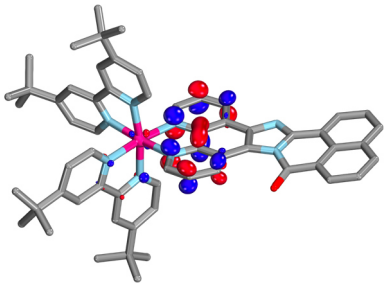

LUMO+1

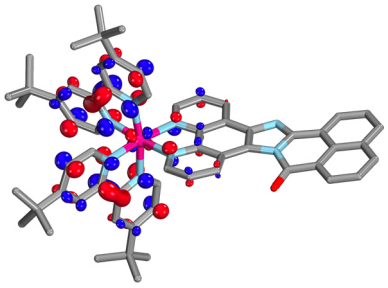

LUMO+2

Figure S9.4. Presentation of the orbitals of complex **Rubiipo** at B3LYP-D3(BJ)/def2-TZVP level of theory. Their contributions to the respective transitions are summarized in Table S9.2.